Amazonian Deforestation and Regional Climate Change

CARLOS A. NOBRE,* PIERS J. SELLERS AND JAGADISH SHUKLA

Center for Ocean–Land–Atmosphere Interactions–COLA, University of Maryland, College Park, Maryland

(Manuscript received 7 December 1990, in final form 29 April 1991)

ABSTRACT

Large-scale conversion of tropical forests into pastures or annual crops could lead to changes in the climate. We have used a coupled numerical model of the global atmosphere and biosphere (Center for Ocean–Land–Atmosphere GCM) to assess the effects of Amazonian deforestation on the regional and global climate. We found that when the Amazonian tropical forests were replaced by degraded grass (pasture) in the model, there was a significant increase in the mean surface temperature (about 2.5°C) and a decrease in the annual evapotranspiration (30% reduction), precipitation (25% reduction), and runoff (20% reduction) in the region. The differences between the two simulations were greatest during the dry season. The deforested case was associated with larger diurnal fluctuations of surface temperature and vapor pressure deficit; such effects have been observed in existing deforested areas in Amazonia. The calculated reduction in precipitation was larger than the calculated decrease in evapotranspiration, indicating a reduction in the regional moisture convergence. There was also an increase in the length of the dry season in the southern half of the Amazon Basin, which could have serious implications for the reestablishment of the tropical forests following massive deforestation since rainforests only occur where the dry season is very short or nonexistent. An empirical bioclimatic scheme based on an integrated soil moisture stress index was used to derive the movement of the savanna–forest boundary in response to the simulated climate change produced by large-scale deforestation. The implications of possible climate changes in adjacent regions are discussed.

1. Introduction

The distribution of global vegetation has traditionally been thought to be determined by local climatic factors, primarily precipitation, radiation, and temperature, and by soil properties, in particular water-holding capacity. For instance, the accepted bioclimatological view holds that rainforests can exist only in high rainfall tropical areas having short or nonexistent dry seasons where soil physical properties ensure high levels of available soil moisture throughout the year. In turn, the mechanisms giving rise to semicontinuous and high rainfall rates throughout the year for those regions were thought to be due solely to the general circulation of the atmosphere and not dependent on the underlying vegetation. This view has been modified in the last 15 years as controlled numerical experiments with complex models of the atmosphere showed that the presence or absence of vegetation can influence the regional climate (e.g., Charney et al. 1977; Shukla and Mintz 1982; Sud and Molod 1988; Sato et al. 1989a; and a review of GCM experiments of land surface processes in Mintz 1984 and Rowntree 1988). One implication of these results is that the current climate and vegetation coexist in a dynamic equilibrium that could be altered by large perturbations in either of the two components.

Deforestation is rapidly progressing in Amazonia. Figure 1 shows deforestation rate estimates in the Brazilian portion of Amazonia from several sources (Brasil 1989; Fearnside 1990; Fearnside et al. 1990; Skole et al. 1990): areas of active development, such as in Rondonia and the Brazilian western Amazonia, are associated with the highest deforestation rates (Malingreau and Tucker 1988; Fearnside 1987a). Other Amazonian countries such as Peru (Gentry and Lopes-Parodi 1980), Colombia, Venezuela, and Bolivia (Myers 1982) also have high rates of deforestation. It is expected that future deforestation rates will be higher because of development policies of the Amazonian countries. If deforestation were to continue at this rate, most of the Amazonian tropical forests would disappear in less than 100 years. One question that arises is whether the large-scale deforestation in Amazonia might affect the regional climate with consequent implications for the biota in the region.

The equilibrium climate is determined by complex interactions among the dynamical processes in the atmosphere and thermodynamic processes at the earth–

* Permanent affiliation: Centro de Previsão de Tempo e Estudos Climáticos-CPTEC, Instituto de Pesquisas Espaciais-INPE, 12201 São José dos Campos, SP, Brazil.

Corresponding author address: Piers J. Sellers, Center for Ocean–Land–Atmosphere Interactions, University of Maryland at College Park, 2213 Computer and Space Science Bldg., College Park, MD 20742-2425.

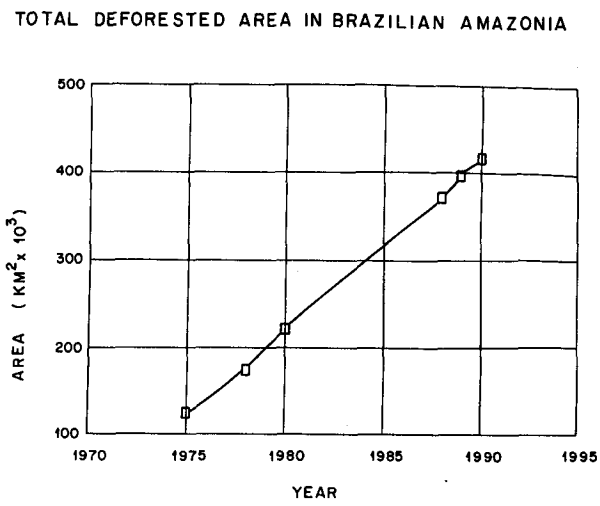

FIG. 1. Estimates of total deforested area in Brazilian Amazonia. Estimates for 1975, 1978, 1988, and 1989 were based on Landsat imagery (Brasil 1989, Fearnside et al. 1990, Skole et al. 1990). Estimates for 1980 and 1990 were based partly on Landsat imagery and partly on linear projections of deforestation (Fearnside 1989). All estimates refer only to deforestation in the tropical forest biome.

atmosphere interface. Therefore, quantitatively estimating the effects that large changes in terrestrial ecosystems can have on temperature, circulation, and rainfall has been a difficult task. Results of early model studies on the effects of deforestation on climate were generally inconclusive, and sometimes conflicting. Two types of models were used: either energy-box models (Potter et al. 1975; Lettau et al. 1979) or coarse resolution GCMs (Henderson-Sellers and Gornitz 1984). In general, these models lacked adequate spatial resolution and realistic treatment of land surface processes. Model horizontal resolutions were typically 10° longitude by 5° latitude which would reduce the whole of Amazonia to four or five grid points. Also, their representations of evapotranspiration processes were based on simple parameterizations. In Henderson-Sellers and Gornitz (1984) runoff was proportional to soil moisture and to the precipitation. These parameterizations, including the "bucket hydrology" (Manabe 1969) parameterization, were inadequate to represent evapotranspiration processes over vegetated surfaces (Sellers et al. 1986) and cannot be used to represent the complex changes in soil hydrology (see section 3) following burning and land clearance.

Realistic models of the biosphere that can be coupled with realistic models of the global atmosphere have only recently been developed (Dickinson et al. 1986; Sellers et al. 1986). Dickinson and Henderson-Sellers (1988, hereafter referred to as DHS) have conducted the pioneering work of assessing climate impacts of tropical deforestations using these improved coupled biosphere–atmosphere models. In DHS the National Center for Atmospheric Research Community Climate Model (NCAR CCM), coupled to the Biosphere–Atmosphere-Transfer-Scheme (BATS), was used with a horizontal resolution of 7.5° × 4.5° to study the impacts of Amazonian deforestation. When the model's rainforests over Amazonia were replaced by degraded pasture, the calculated surface temperatures increased and evapotranspiration decreased over the region. The increase in surface temperature was attributed mostly to the decreased roughness length of the grass vegetation compared to that of forest and the reduction of evapotranspiration to the reduction in the amount of absorbed solar radiation for grass, a result primarily due to its higher albedo. On the other hand, the calculated rainfall decreased in some parts of Amazonia but increased in other parts. Some difficulties were reported in the parameterizations of incident solar radiation and interception loss (Shuttleworth and Dickinson 1989; Dickinson 1989a,b) that caused unrealistically high evapotranspiration rates. More recently a GCM simulation of tropical deforestation was conducted at the U.K. Meteorological Office (Lean and Warrilow 1989, hereafter referred to as LW). The model's horizontal resolution was 3.75° × 2.5° and all the model's vegetation north of 30°S in South America was replaced by grass. Their results were similar to those in DHS: surface temperature increased and evapotranspiration decreased for the pasture scenario compared to the forest one. Additionally, it was found that simulated precipitation was reduced over Amazonia. As in DHS the increase in surface temperature was attributed to the decrease in roughness length and the decrease in evapotranspiration to the reduction in the amount of absorbed solar radiation for grass due to its higher albedo.

The observed distribution of precipitation in tropical South America shows large areas where annual values reach 3000 mm or more. On the eastern Andean slopes and on the western coast of Colombia, annual totals in excess of 5000 mm are due mainly to the mechanical uplifting of the low-level airflow by the topography; along the Atlantic coast from Guianas to the state of Maranhão, in Brazil, westward-propagating sea-breeze squall lines (Kousky 1980; Cohen et al. 1989) account for the observed large precipitation values (in excess of 3000 mm annually); the reasons for the broad precipitation maximum found over the western part of Amazonia are not well understood, but there has been a suggestion (Nobre 1983; Salati and Vose 1984) that the concave shape of the Andes Mountains to the west of the precipitation maximum may favor convergence of the low-level, predominantly easterly, moisture-laden flow. Besides these features, there is an elongated secondary precipitation maximum, where annual values are above 2000 mm, extending from southwestern Amazonia toward the southeast and joining with the high precipitation area of the South Atlantic convergence zone (SACZ). This secondary maximum marks the northernmost position of frontal systems propa-

gating equatorward from midlatitudes of the Southern Hemisphere and is a preferred position for frontal systems to remain quasi-stationary (Kousky 1979; Oliveira and Nobre 1986). The dynamics of the interactions between these frontal systems and tropical convection is not well understood.

The mechanisms that explain the various precipitation maxima mentioned above are apparently linked to the general circulation of the atmosphere or to local or mesoscale forcing (topographic uplifting, diurnal land–sea temperature contrast), and are not primarily dependent on the underlying vegetation cover. It is likely that precipitation maxima would exist in those areas even in the absence of the rainforest (although perhaps at a different intensity and temporal distribution). Indeed, the paleoclimatic record for Amazonia suggests that during glaciation peaks, most of the region was covered by savanna and the rainforest retreated to areas that broadly coincided with the current spatial occurrence of precipitation maxima (Dickinson and Virji 1987; Whitmore and Prance 1987; Salo 1987; Colinvaux 1987, 1989). The association between the areas where the rainforest retreated (refuges) and high precipitation appears to be reasonable because rainforests exist only in places with high rainfall rates and short dry seasons (Prance 1986).

This line of reasoning suggests that the vegetation in the region plays a secondary role as a climate-forcing factor. However, there is a wealth of observational evidence pointing otherwise, namely: (i) on the basin-wide scale, several independent calculations of actual evapotranspiration (see a review of these calculations in Salati and Nobre 1990) and the water balance for the Brazilian Amazonia during the period April–May 1987 (Table 1) all show that evapotranspiration accounts for more than 50% of the precipitation. As indicated in Table 1, the precipitable water in the atmospheric column for a station in western Amazonia (Tabatinga), 2500 km from the Atlantic coast, is higher than for a station near the coast (Belem), showing that there is a moistening of the lower troposphere as the air flows over the forested surface, presumably due to water vapor recycling by the vegetation; (ii) water balance calculations for small watersheds in the region ranging from 1.3 to 23.5 km^2 have also shown that evapotranspiration accounts for more than 50% of precipitation (Franken and Leopoldo 1984); (iii) an evapotranspiration model constructed from measurements at a micrometeorological tower near Manaus, Brazil, for more than two years (Shuttleworth 1988) showed an average flux of water vapor into the atmosphere of 3.6 mm day^{-1} whereas the average precipitation was 7.2 mm day^{-1}; (iv) the difference in surface properties between forest and large rivers (>5 km in width) may favor precipitation over forested surfaces rather than over water, as indicated by the observations of Molion and Dallarosa (1990) who reported that over a ten-year period, raingages on river islands located in the Amazon River and in large tributaries recorded less precipitation than raingages located in the adjacent forest.

Taken together, all the available observational evidence seems to suggest that the Amazonian rainforest is highly efficient in recycling precipitation water into the atmosphere. The results of this study show that a degraded pasture cover, which could take the place of the forest, could not maintain such a high evapotranspiration rate (for reasons discussed in sections 3a, 4a, and 4c). This, with other changes, may indicate the existence of a significant sensitivity of the regional climate to the presence or absence of the tropical forest.

Removal of the Amazonian forest could also have tremendous effects on species diversity and atmospheric chemistry (Houghton et al. 1985). The Amazon basin is host to roughly half of the world's species, and the intensity and complexity of plant–animal interactions (Mori and Prance 1987) and the rapid nutrient cycling in the soils (Dias and Nortcliff 1985) make the region vulnerable to disturbance. The Amazon is also an important natural sink of ozone and plays an important role in global tropospheric chemistry, including the injection of large amounts of CO_2 into the atmosphere from biomass burning (Fearnside 1987b; Crutzen and Andreae 1990). However, the

TABLE 1. Atmospheric water balance for the Amazon Boundary Layer 2B (ABLE-2B) Experiment: one-month (13 April–13 May 1987) averaged values for an area of 2.2×10^6 km^2 in Brazilian Amazonia; calculation of terms A and B was based on four-times-per-day upper air sounding data for six upper air stations listed; average precipitation (term D) was based on daily precipitation totals for 90 surface stations, and average evapotranspiration (term C) was calculated as a residual of the atmospheric water balance equation.

	Water balance terms		Station	Latitude	Longitude	Precipitable water (mm)
A	Time rate of change of precipitable (storage term)	−0.2 mm day^{-1}	Belem	1.38°S	48.48°W	56.8
			Boa Vista	2.83°N	60.67°W	61.7
			Tabatinga	4.17°S	69.75°W	61.6
B	Divergence of the vertically integrated moisture transport	−4.2 mm day^{-1}	Vilhena	12.73°S	60.13°W	44.6
			A. Floresta	9.45°S	56.25°W	51.6
			Manaus	2.55°S	59.97°W	60.5
C	Evapotranspiration	5.3 mm day^{-1}				
D	Precipitation	9.7 mm day^{-1}				

present study is mainly confined to the assessment of the effects of deforestation on the physical climate system.

In this paper, we describe the use of a coupled atmosphere–biosphere model to investigate the consequences of the removal of Amazonian forests on climate. Some initial results of this study were presented in Shukla et al. (1990).

2. Description of model

a. The model

The model used in this investigation is a modified version of the National Meteorological Center (NMC) global spectral model. The dynamic formulation of the model is described in Sela (1980) and the initialization procedures and boundary conditions are described in Kinter et al. (1988). The model has a rhomboidal truncation at total wavenumber 40 (equivalent approximately to a resolution of 1.8° × 2.8°) and is discretized into 18 vertical layers. Temperature and winds are defined in all the model's 18 layers but specific humidity is only defined for the lowest 12 layers (see Kinter et al. 1988).

The physics include: (i) the efficient radiation scheme of Harshvardhan et al. (1987) to permit the simulation of the diurnal cycle. The parameterization for the transfer of shortwave radiation is based on Lacis and Hansen (1974) as modified by Davies (1982), and the radiative transfer calculations for the longwave component of terrestrial radiation are based on the scheme of Harshvardhan and Corsetti (1984); (ii) a boundary-layer momentum and heat flux parameterization based on the similarity theory of Monin–Obukhov (1954) as used in the E2-Physics package of the Geophysical Fluid Dynamic Laboratory (GFDL) model (Miyakoda and Sirutis 1986); (iii) a modified Kuo scheme for convection and large-scale precipitation (Sela 1980, after Kuo 1965, and Philips 1979), and a shallow convection scheme (Tiedke 1984); (iv) the parameterization for vertical diffusion of momentum, heat and moisture in the PBL, based on the level 2 second-order closure model of Mellor and Yamada (1982), and a biharmonic diffusion (Laplacian) operator used for horizontal diffusion on constant sigma-surfaces to avoid spectral blocking.

The large-scale topography and sea surface temperature (SST) fields are prescribed. Prescribed zonally symmetric ozone mixing ratios and cloudiness derived from observed seasonal mean values are used in the radiative transfer calculations.

Further modifications to the model physics, including the coupling of the GCM to the biosphere model, are summarized below and described in greater detail in Sato et al. (1989a,b).

b. Simple biosphere model (SiB)

Until the early 1980s, all the land surface parameterizations (LSPs) used in GCMs were based on the so-called bucket model (Budyko 1974; Manabe 1969), in which albedos and surface roughness lengths were specified as independent parameters for terrestrial grid areas and the partitioning of absorbed radiative energy into sensible and latent heat fluxes was determined as a simple function of "soil moisture."

Starting with the models of Dickinson (1984) and Sellers et al. (1986), biophysically based LSPs have been designed and implemented in many GCMs. These models attempt to describe the biophysical controls on the exchange of radiation, momentum, and heat flux by modeling the vegetation itself so that these exchange processes are mutually consistent. The Simple Biosphere model (SiB) of Sellers et al. (1986), implemented in the COLA-GCM, makes use of a database that divides the world into 12 biomes (see Fig. 2 for specification of biomes for South America), each with its soil and vegetation characteristics specified in some

FIG. 2. Distribution of SiB vegetation types on the Gaussian grid over South America used in the control case: 1—broadleaf evergreen (*tropical forest*), 2—broadleaf deciduous, 3—mixed broadleaf deciduous and needleleaf evergreen, 4—needleleaf evergreen, 5—needleleaf deciduous, 6—grass and broadleaf deciduous shrubs, 7—grass, 8—broadleaf deciduous shrubs, growing singly, in patches or groups, 9—broadleaf deciduous shrubs, growing singly or in patches (semi-desert), T—tundra, D—desert, C—cultivated land represented by wheat, and *—glacier or permanent land ice cover.

detail. Radiative transfer is modeled using a two-stream approximation model in which the optical and geometric properties of the leaves and stems and the optical properties of the soil are used to calculate the surface albedo and the attenuation of photosynthetically active radiation (PAR) down through the canopy. A first-order closure model, calibrated against a second-order closure model, is used to define surface roughness length and the aerodynamic resistances between the canopy, soil surface, and canopy air space as functions of the vegetation height, foliage density, and morphology. Last, an empirical physiological model, based on the work of Jarvis (1976), is used to calculate the bulk canopy resistance, that is, the diffusion resistance imposed by the microscopic pores (stomata) in leaf surfaces as a function of vegetation type, leaf area index and greenness, absorbed PAR, temperature, humidity, and soil moisture potential. This canopy resistance is the dominant term in regulating the evapotranspiration rate of a dry canopy (see Sato et al. 1989a).

A simple isothermal scheme is used to describe the transfer of water between the three model soil layers due to hydraulic diffusion and gravitation. The rate of transfer is dependent on the product of the gradient of soil moisture potential, φ, plus gravitation and the mean (between-layer) hydraulic conductivity, K. Both K and φ are highly nonlinear functions of soil moisture content with controlling parameters governed by soil physical properties. Sandy soils and soils with organic matter content tend to have high hydraulic conductivity and are associated with lower surface runoff rates. Clay soils with low organic matter content can have very low hydraulic conductivities and are usually associated with poor percolation rates and reduced soil evaporation rates. There are three soil layers in the model: a thin evaporating upper layer, the root zone, and a recharge zone. The model canopy is capable of storing around 1 mm of intercepted rainfall, which is available for free evaporation back to the atmosphere. In the SiB-GCM study of Sato et al. (1989a), interception loss for an area around Manaus was estimated to make up roughly 28% of the total evapotranspiration loss during June–July.

The effects of the spatial nonuniformity of convective precipitation are dealt with very simply in SiB-GCM. An empirical area-intensity function is used so that a large fraction of convective rainfall is concentrated within a relatively small proportion of the grid area, so that most of it falls through the canopy; if the local soil infiltration rate is exceeded, this throughfall may contribute to surface runoff (see Sato et al. 1989b).

The Simple Biosphere model has been extensively tested offline (Sellers and Dorman 1987; Sellers et al. 1989; Dorman and Sellers 1989). The model was calibrated for tropical forests using the meteorological and flux measurements of Shuttleworth et al. (1984) for an instrumented site near Manaus, Brazil. Some of the physiological constants used to describe stomatal functioning in SiB were adjusted to provide the best match between observed and calibrated fluxes. To date, this procedure has not been done for any other biome.

The Simple Biosphere model has been implemented in the COLA-GCM and its performance compared to that of preexisting bucket hydrological models by Sato et al. (1989a). The atmospheric state variables in the model such as temperature, specific humidity, and wind velocity were coupled with the SiB "fast" prognostic variables (canopy and ground cover temperatures), using an implicit time integration scheme to maintain numerical stability and conserve energy. The other SiB prognostic variables are slowly varying and a forward scheme is used for the integration (Sato et al. 1989a).

In general, the SiB-GCM combination calculated more realistic values of the surface heat fluxes, near-surface air temperature, humidity, and boundary-layer height both in terms of magnitude and diurnal variation. In SiB-GCM, the wind speed, air temperature, incident radiative flux, and precipitation as calculated by the atmospheric GCM are used to force the SiB component, which then predicts the time rate of change of the SiB variables: canopy temperature; ground temperature; deep soil temperature; liquid water stored on canopy foliage and ground cover foliage; and the wetness of the soil surface layer, root zone, and recharge zone. Runoff, soil moisture, and sensible and latent heat fluxes are calculated as diagnostic outputs of the SiB and are passed back to the GCM.

The version of SiB used in the study of Sato et al. (1989a) is essentially the same as the one used here with some minor modifications to the calculation of runoff, soil evaporation, and the distribution of vegetation in South America. The soil evaporation component of the model was changed from the original version as described in Sellers et al. (1986). First, the results of Camillo and Gurney (1986) were used to curve-fit a simple relationship between soil surface resistance and wetness of the upper 0.5 cm of the soil. The relationship is significantly different from the formulation of Shu Fen Sun (1982) used previously in SiB. Second, the wetness of the top 0.5 cm of soil is calculated from the wetness of the first two soil layers, typically 2 cm thick and 40 cm thick, assuming a uniform flux throughout the profile and reduced hydraulic conductivity right near the soil surface, in accordance with observations of the effect of rain impacts, mechanical compaction, and clay "caking" following evaporation.

The original global vegetation cover description used in SiB is described in Dorman and Sellers (1989). On close inspection, this was found to contain some geographical inaccuracies for South America, primarily in the location of some of the boundaries of the tropical forests, which were corrected using the $1° \times 1°$ global compilation of vegetation types by Matthews (1985), the RADAM (radar mapping) vegetation maps for Brazil (Brasil 1980), and the satellite-derived vegetation indices for South America (Justice et al. 1985).

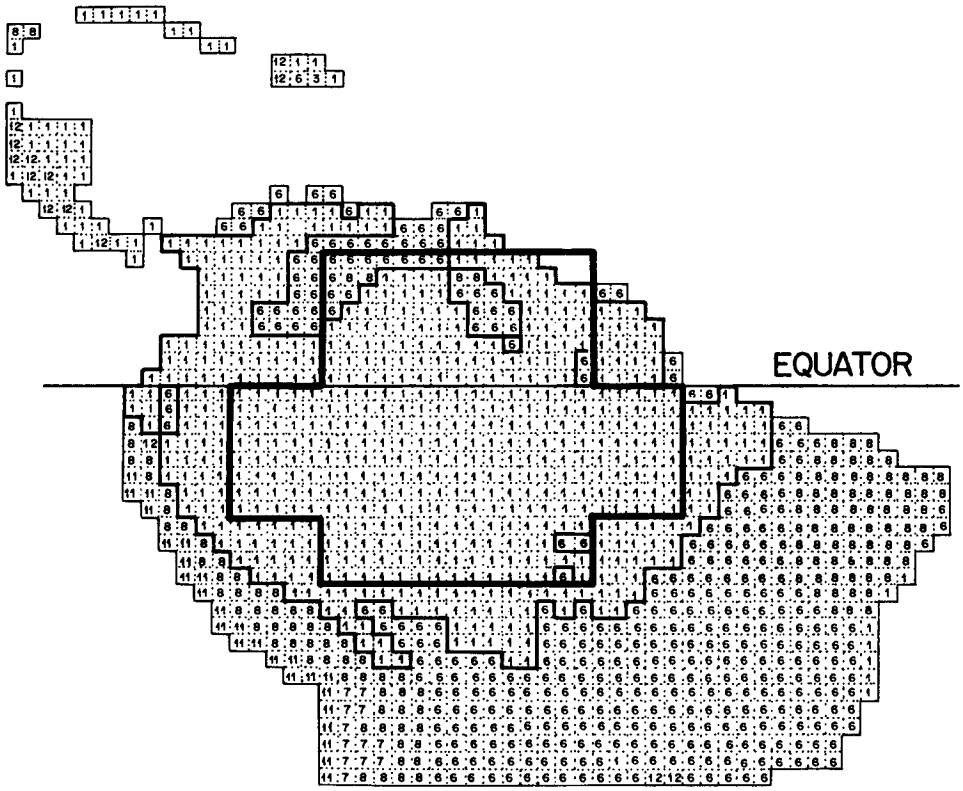

FIG. 3. Distributions of SiB vegetation types over tropical South America on a 1° by 1° long grid. The area of the Amazon tropical forests are encircled by the solid lines. The vegetation types are described in Fig. 2. The two areas shown (box I: northern Amazonia and box II: southern Amazonia) were used for areal averages as indicated in the text.

The resulting 1° × 1° vegetation map for South America is shown in Fig. 3.

3. Description of experiments and experimental design

a. Deforestation scenarios

The "control" experiment of this study was conducted using the tropical forest with the SiB ecophysiological and morphological parameters derived from the dataset of Shuttleworth et al. (1984), as described in Sellers et al. (1989) and tested in the GCM in Sato et al. (1989a). Their results show that the "undisturbed" tropical forest scenario is reasonably well simulated in this study.

The definition of the surface parameters for the deforested case is more problematical as there are a number of different fates for deforested areas. These include regrowth back to secondary forest, agriculture, pasture, and ultimately abandoned pasture or agriculture. We have chosen the abandoned pasture scenario to represent the deforested case as this is the most extreme option (we do not consider bare soil to be a realistic scenario) in terms of land degradation, on the grounds that if the regional climate shows no sensitivity to this degree of land surface change, then no intermediate scenarios need be studied. Additionally, observations of land use patterns in Amazonia show that most of the primary forest being cleared is replaced by pasture (Fearnside 1987a). Nutrient-poor soils and poor pasture management practices accelerate the degradation of soil and vegetation cover, causing its abandonment after a few years of use. This is typically the case for most of the Zona Bragantina (area about 30 000 km^2), just northeast of Belem, near the mouth of the Amazon River, which was deforested in the first two decades of this century and where there has never been extensive regrowth of the natural vegetation (Fearnside 1982). An example of abandoned pasture typical of the scenario used in this simulation is shown in the photograph of Fig. 4.

The characteristic parameter values for the degraded pasture scenario of this study were based on observations reported in the ecological literature. The pasture is represented as a mixed herbaceous community dominated by C_4 species (typical species would include *Panicum maximum, Andropogon gayanis, Bracharia humidicola*) with maximum green leaf area indices of around 2, total leaf area index of 4 (Nepstad and Uhl

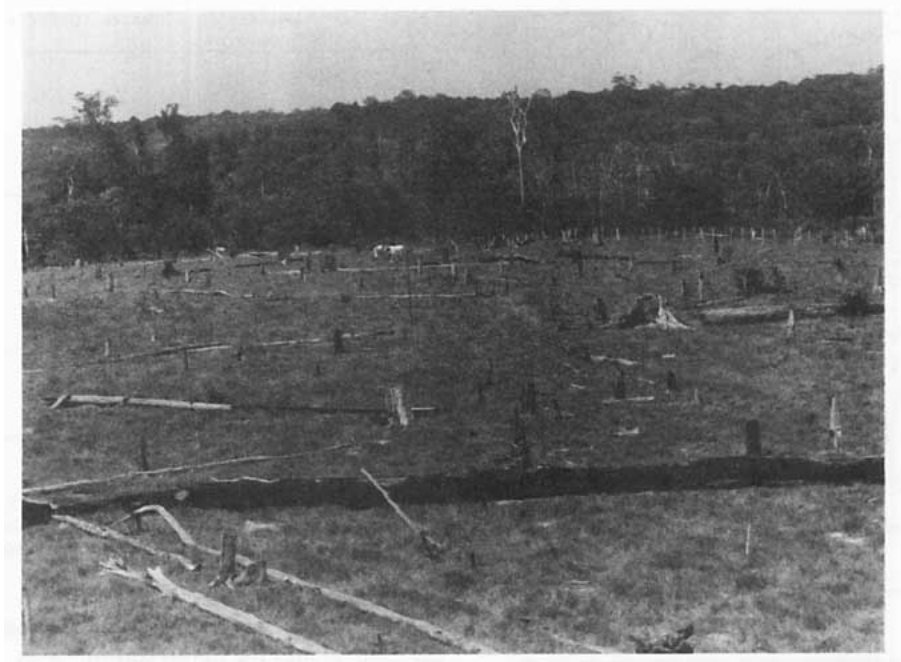

FIG. 4. Photograph of an area in central Amazonia, 100 km north of Manaus, (approximately at 2.0°S, 60°W) showing a typical pasture in Amazonia. Secondary forest bordering the pasture appears in the background.

1990). The optical and morphological properties of this grassy vegetation cover are assumed to be the same as for temperate grasses and are therefore specified as described in Dorman and Sellers (1989). In its final form, the vegetation cover consists of a mat of dead foliage, covering 85% of the soil surface, with protruding live and dead foliage extending up to a height of 60 cm. Both forest and pasture scenarios are depicted schematically in Fig. 5.

The physiological characteristics of the grasses were taken from the reports of Bjorkman (1981) and Korner et al. (1979) for the light response characteristics, and Ludlow and Ibaraki (1979), Ng et al. (1975), and Ludlow and Wilson (1971a,b, 1985) for the humidity and the leaf-soil moisture dependencies (see Fig. 6 and Table 2). Interestingly, while the grass and forest canopies are calculated to have similar minimum resistances, the grass cover is assigned a stronger response to vapor pressure deficits: the forest canopy stomates would be completely closed at a vapor pressure deficit of 60 mb, the grass at 52 mb.

The most drastic differences between the characteristics assigned to the two covers occur below the surface. Table 2 shows root length, root depth, and soil physical properties. The pasture has a shallower, sparser root system, 0.6 m compared to 2.0 m, following the data of Dias Filho (1987), with the result that the pasture cannot access some of the deeper soil moisture. The soil physical properties are also very different. The findings of Medina (1985) and Chauvel et al. (1988) indicate that the degraded pasture typically has a hydraulic conductivity ten times smaller than that of the undisturbed forest. In nature, this is associated with a severe deterioration in the soil structure following burning and land clearance. The undisturbed forest has small amounts of phosphate stably bound with Fe and Al for normal (undisturbed) conditions of low soil acidity. After clearing and burning, the acidity of the soil decreases, causing the release of cations; the phosphate is released into the soil; and the crops or herbaceous species thrive for a couple of years due to the temporary increase in fertility. Thereafter, the cations are progressively leached from the system, soil acidity increases, phosphates become unavailable, and the buffering capacity of the dwindling supply of organic material is reduced so that the clay structures are disaggregated and dispersed. This collapsed soil structure has physical properties more like a clay than the loamy properties of the forest (see Prance and Lovejoy 1984; Jerry 1986; Wilding et al. 1983; Uhl et al. 1988; Buschbacher et al. 1988; and Shubart 1977). The net result is a soil that holds less water available to vegetation and has a low hydraulic conductivity (infiltration rate) at the surface.

One other modification was made to the model to account for soil evaporation effects. It has been noted that repeated trampling and exposure of the soil surface in such pastures leads to the formation of a thin surface layer of reduced permeability (Buschbasher et al. 1988; Jordan 1984). In calculating the surface water content

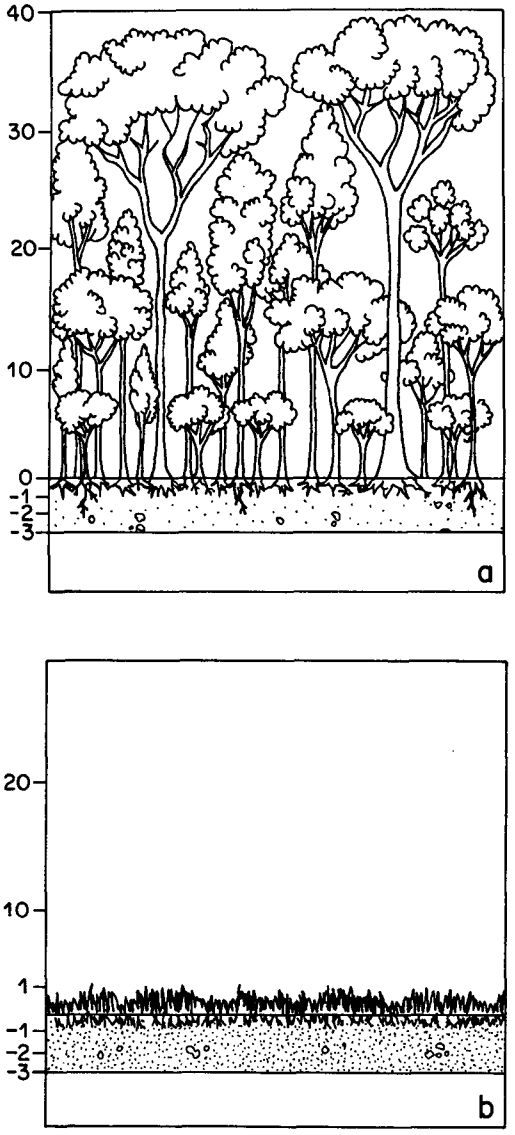

FIG. 5. Schematic diagram depicting the morphologies of (a) the forest and (b) degraded pasture scenarios used in the study.

for the soil evaporation model, it was assumed that the hydraulic conductivity in the top 1 cm of soil was reduced to roughly 1/20 of its value within the bulk soil.

b. *Experimental design*

We first integrated the coupled atmosphere–biosphere model for one year with the normal prescribed global climatological boundary conditions of vegetation distribution, in which the Amazonian region is covered with tropical forests. We refer to this integration as the *control case.* We then repeated the integrations for one year in which all the previous global climatological boundary conditions remained the same except over Amazonia, where the tropical forests were replaced by the degraded pasture cover described above; we refer

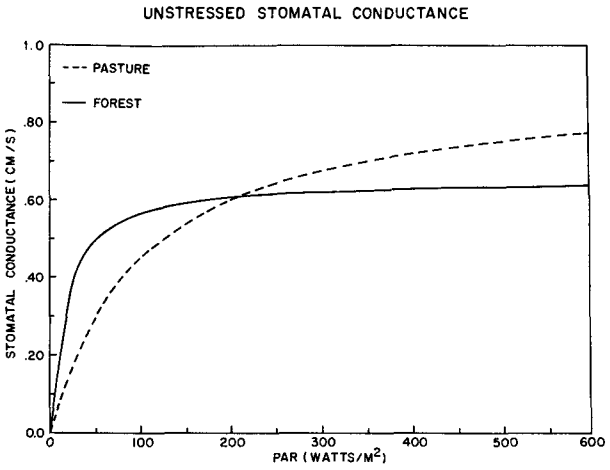

FIG. 6. Unstressed stomatal conductance ($1/r_s$) responses for green leaves as a function of photosynthetically active radiation (PAR) for the tropical forest and degraded pasture vegetation.

to this integration as the *deforestation case.* In both the control and the deforestation cases, the global SST distributions remained inadvertently fixed for the whole integration period and corresponded to the climatological mean values for December. This error is common to both simulation runs, but it appears that comparisons between the two simulations are still valid for studying the model's regional climate sensitivity to

TABLE 2. Comparison of SiB parameters for the tropical forest and degraded pasture vegetation types.

	Tropical forest	Degraded pasture
(a) Vegetation properties		
Albedo* (%)	12–14	16–24
Roughness length* z_0 (m)	2.65	0.08
Displacement height d (m)	27.4	0.25
Minimum canopy resistance* (sm^{-1})	33.9	55.0
Root depth (m)	2.0	0.6
Maximum total root length (m^{-1})	2×10^4	1×10^4
Canopy height (m)	35.0	0.6
Maximum total leaf area index	5.0	4–5
Maximum green leaf area index	4.5	2.2
Fractional area covered by vegetation	1.0	0.85
(b) Soil properties		
Total soil depth (m)	3.5	3.5
Porosity, θs	0.42	0.42
Saturated hydraulic conductivity, K_s (m s^{-1})	2×10^{-5}	2×10^{-6}
Soil moisture potential at saturation, ψs (m)	−0.086	−0.153
B-factor (B) relating soil potential, ψ, to wetness, W ($\psi = \psi_s W^{-B}$)	7.12	10.4

changes in vegetation cover in Amazonia, since the seasonal cycle was reasonably well simulated in that region (see section 4a).

The model integrations were started from the atmospheric state on 1200 UTC 15 December 1986 and integrations were carried out for 12.5 months. This initial date was chosen so that the initial soil moisture in the region could be assumed to be at or near saturation in both cases, since the initialization of the soil moisture field is difficult due to the relatively long "memory" of the soil moisture store (see Sellers et al. 1986; Dorman and Sellers 1987; and appendix D of Sato et al. 1989b for a discussion on the problems of soil moisture initialization in SiB). The resulting simulated fields are compared to investigate the effects of changing the vegetation in Amazonia. Special attention has been given to differences between the surface hydrology and surface energy budgets calculated by the two simulations.

4. Results

a. Comparison of the control simulation and observations

Selected fields of simulated sea level pressure (SLP) and precipitation for tropical South America were compared with observations. Model and observations were in very good agreement for SLP, including its seasonal pattern. Satisfactory agreement was found for precipitation in spite of the difficulty this model and other GCMs have in reproducing the details of the seasonal cycle of precipitation in central Amazonia.

1) SEA LEVEL PRESSURE

Sea level pressure distributions for January and July from the control simulation are compared to the observations reported by Godbole and Shukla (1981) for the same months (Fig. 7). For January the main features of the SLP fields are well represented in the model

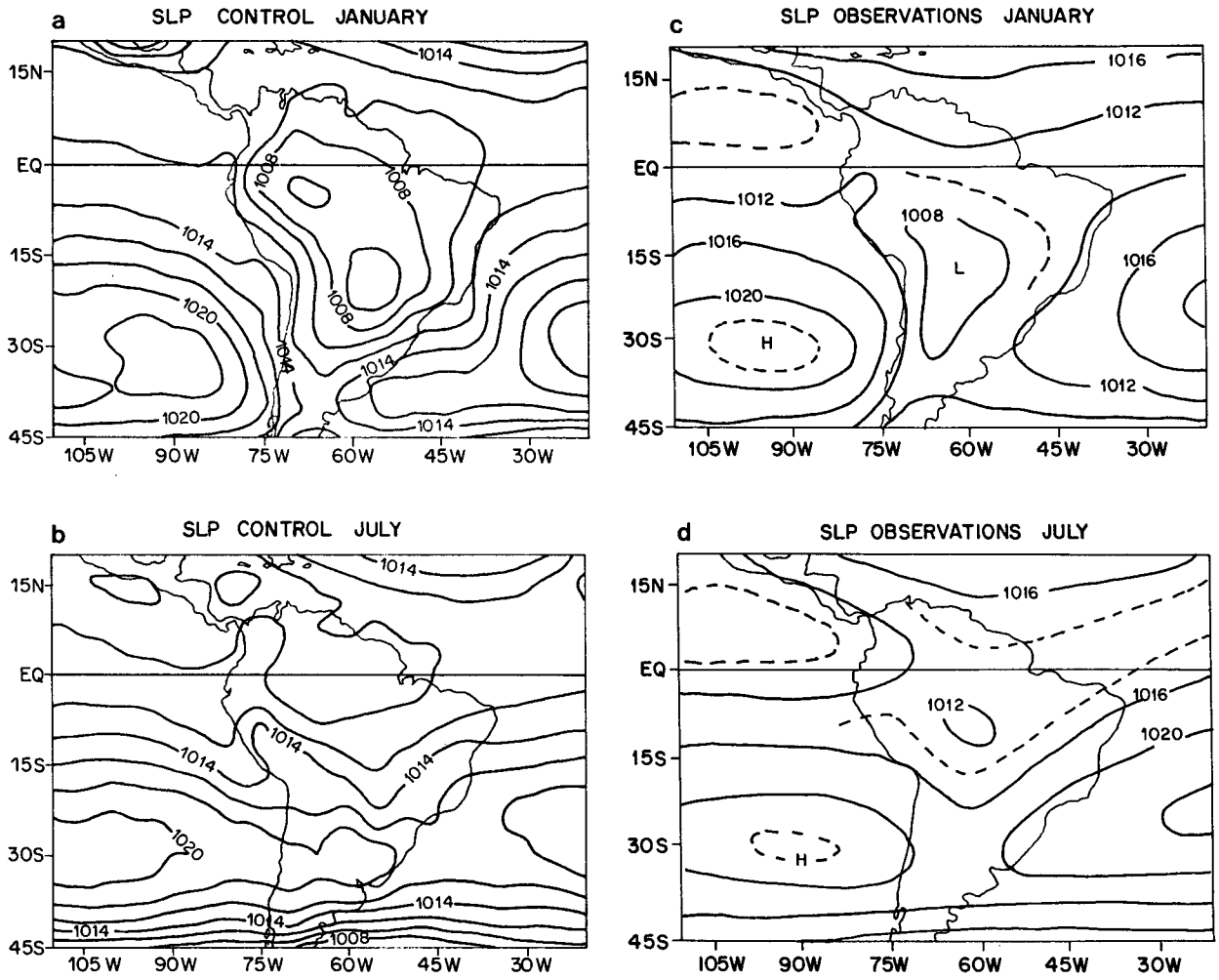

FIG. 7. Sea level pressure distribution for South America (hPa): (a) January and (b) July values from the control simulation (model) and (c) January and (d) July from observations of Godbole and Shukla (1981). Contour interval is 2 hPa in (a) and (b), and 4 hPa in (c) and (d).

simulation: the continental low pressure is deeper in the model simulation by about 2 mb; the SLP distribution of both the southeast Pacific and South Atlantic subtropical highs is similar between model and observations. For July the main observed features were also captured in the model: namely, a zonally oriented SLP distribution over subtropical South America joined with the subtropical highs of both oceans, and the mid-continental trough, which is slightly displaced to the east in the model compared to observations.

2) Monthly total precipitation

Monthly total precipitation distributions for January and July from the control simulation were compared with the observations of Figueroa and Nobre (1990) for tropical South America (Fig. 8). The model realistically reproduces the South Atlantic convergence zone (SACZ), showing a band of maximum precipitation extending from the continent into the South Atlantic Ocean. The model also shows a maximum higher than 12 mm day^{-1} near the coast. Observations (not shown in Fig. 8, see Kousky 1979) show the existence of such a maximum. A deficiency in the simulated (model) precipitation is seen in central Amazonia: simulated values are well below observations, about 4 mm day^{-1} in the former as opposed to 8 to 10 mm day^{-1} in the latter. The simulated precipitation pattern also shows a conspicuous maximum over Central America throughout the year that is not seen in the observations. For July the simulated precipitation decreases markedly for subtropical South America, and the precipitation maximum is found north of the equator. These features are corroborated by observations.

3) Seasonal cycle of precipitation

The seasonal cycle of simulated precipitation is shown for northern Amazonia (Region I) and southern Amazonia (Region II) in Fig. 15a (solid line). The seasonal rainfall distributions for a number of stations from observations of Figueroa and Nobre (1990) is shown in Fig. 9. In this figure the dash-point line encircles all stations in tropical South America for which the dry season is short (less than three months with monthly rainfall smaller than 50 mm). It is remarkable that this line corresponds quite well with the limits of the tropical forest. The large discrepancy between observations and the calculated precipitation for central-southern Amazonia is the simulation of double maxima (March and October) in the rainfall distributions, which are not present in the observations. This problem (simulation of unrealistically low precipitation rates in December and January in central-southern Amazonia) is not thought to have been caused by the time-invariant SSTs, since the SSTs were fixed for December climatological values and it is primarily for December and January that the simulated precipitation does not

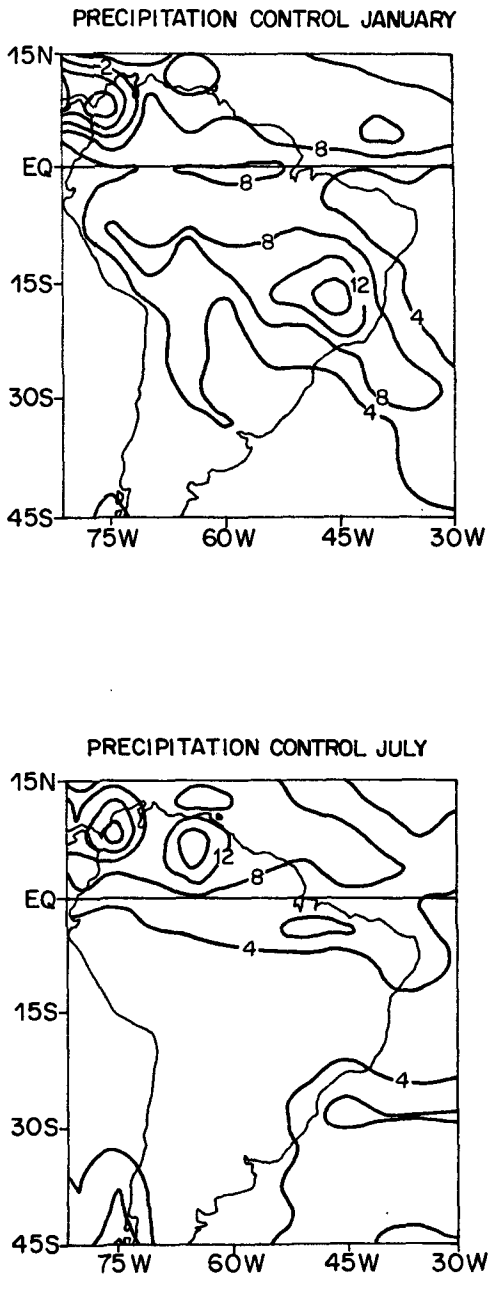

FIG. 8. Precipitation distribution for tropical South America: (a) January and (b) July totals from the control simulation (model) in mm day^{-1} and (c) January and (d) July from observations of Figueroa and Nobre (1990) in mm mo^{-1}.

agree with the observations. Apparently tropical continental convection in the model is mostly triggered by solar heating so that the model's largest precipitation rates occur in central Amazonia in March and October when solar heating peaks at those latitudes. Also, model and observations agree well in capturing the double precipitation maxima in the seasonal cycle of precipitation over equatorial Africa (not shown). The dynamics of the seasonal precipitation distribution over

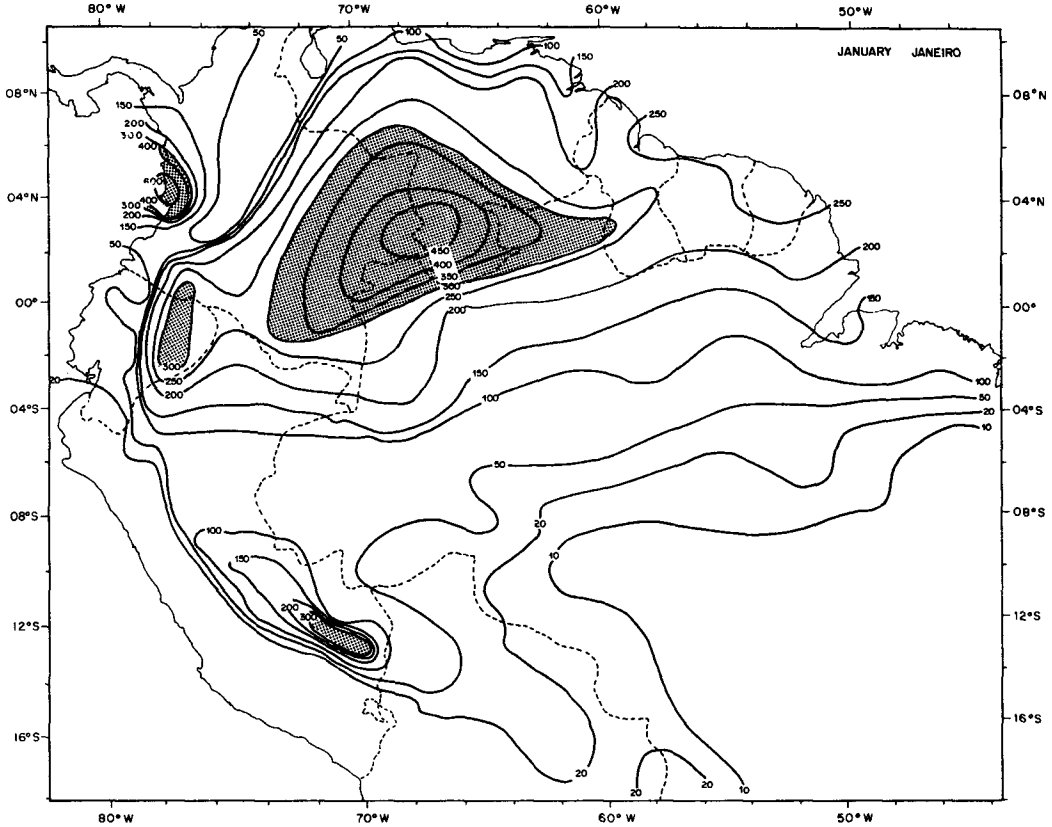

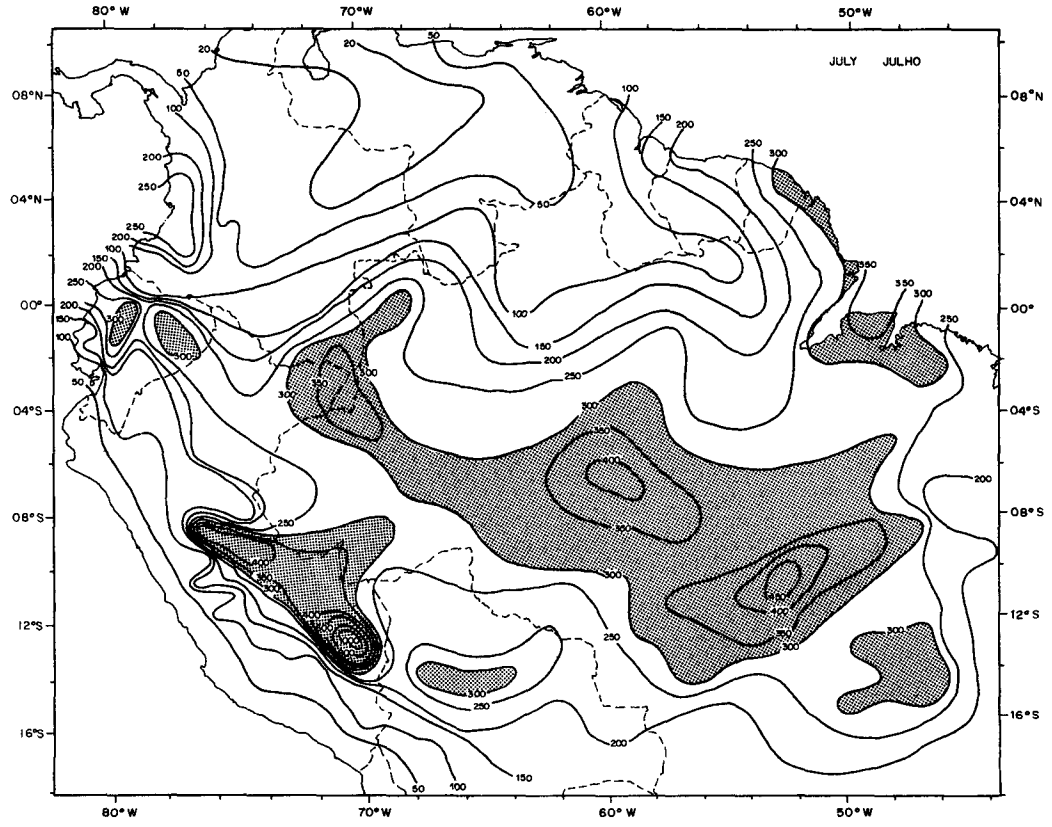

FIG. 8. (*Continued*)

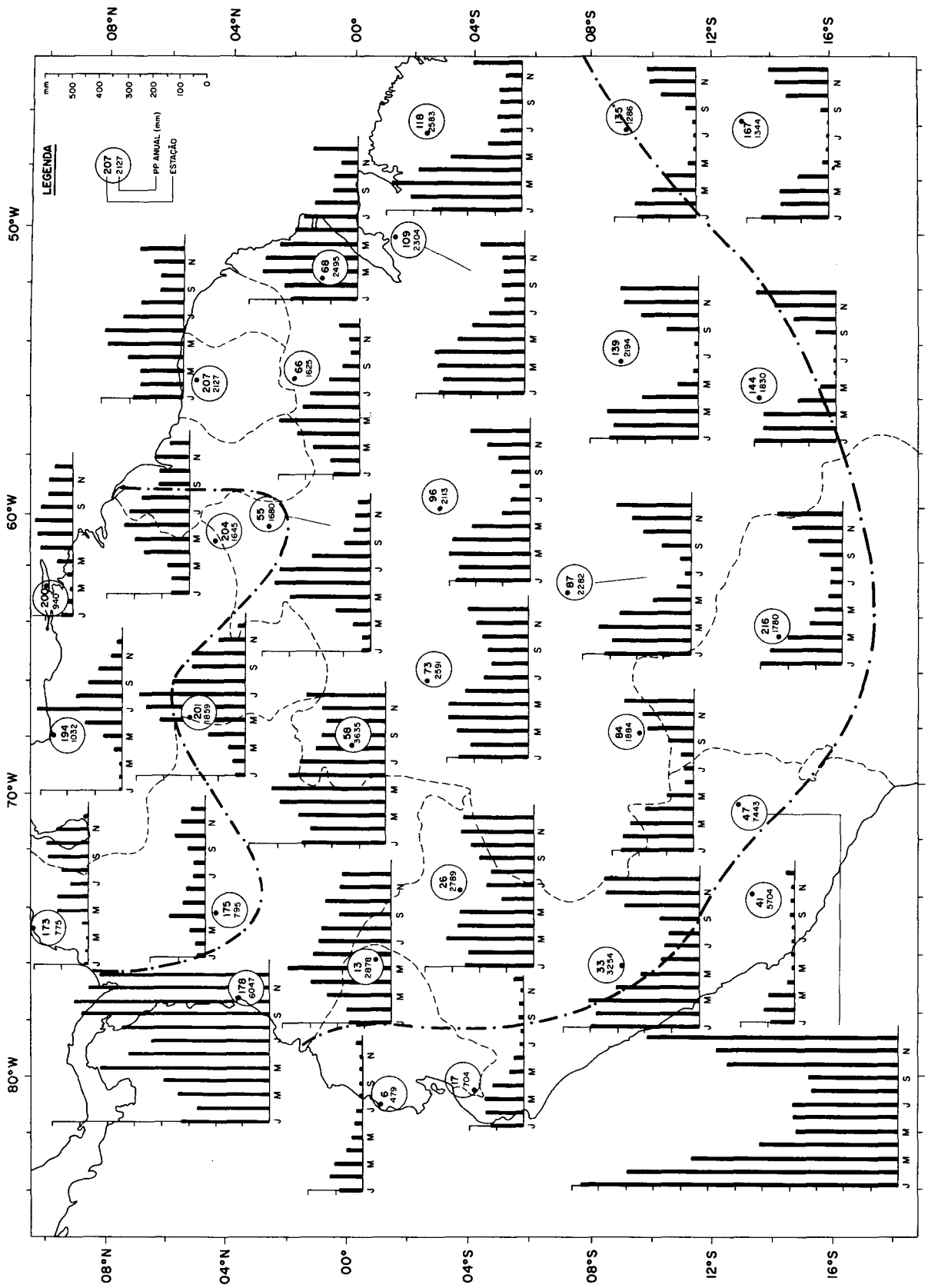

FIG. 9. Annual march of rainfall for several stations in tropical South America from the observations of Figueroa and Nobre (1990). The dash–dot line encircles stations for which the dry season is normally short (less than three months with monthly rainfall lower than 50 mm).

equatorial South America are not as simple as the relatively simple mechanism of meridional ITCZ displacements in equatorial Africa. As discussed in Nobre (1983), the precipitation regimes in tropical South America cannot be understood simply as a response to ITCZ dynamics, and apparently some GCMs are still unable to represent details of the seasonal cycle of precipitation over central Amazonia.

On the other hand, the simulated seasonal cycles of surface temperature and precipitation for the southernmost portion of Amazonia (Fig. 15) and central Brazil (not shown) show a large seasonal contrast in precipitation amounts from the rainy season (austral summer) to the dry season (austral winter), which is supported by observations (see Fig. 9 for the stations in the lower part of the diagram that correspond to the area represented in Fig. 15).

b. Comparison of control and deforestation simulations

The results shown in Figs. 10 through 12 are 12-month averages (1 January to 31 December); the first two weeks of model integration were not used in the analysis.

Soil and surface temperatures are warmer by 1°–3°C in the deforestation case compared to the control case (Figs. 10a,b). This warming extends from the surface throughout the depth of the PBL. At 850 hPa (Fig. 10c) temperatures are 0.5°–1.5°C warmer and specific humidities lower by 1–1.5 g kg^{-1} (Fig. 10d) for the deforested case relative to the control case. A decrease in moisture and an increase in temperature means that PBL relative humidity decreased (by 5%–10% at 850 hPa, Fig. 10e) in the deforestation case relative to the control case. Total precipitation was reduced by 400–800 mm year^{-1} (Fig. 10f), whereas the fluxes of latent heat from the surface decreased (Fig. 11a) by 30–50 W m^{-2} (equivalent to approximately 350–650 mm yr^{-1}) in the deforestation case compared to the control case. To partially compensate for the decrease in latent heating, sensible heat fluxes increased by about 10–20 W m^{-2} in the deforestation case relative to the control case (Fig. 11b); this relative warming of the deforested land surface and the overlying air is consistent with the reduction in evapotranspiration and the lower surface roughness length. This result is in agreement with results of earlier simulation experiments (DHS and LW) and some observations (Shulz 1960; Ghuman and Lal 1987; Lawson et al. 1981) for tropical forests. It should be noted that some of these results are identical to those of Shukla et al. (1990) except that the latter outputs were further smoothed.

The changes in large-scale precipitation are reflected in the dynamical fields since condensational heating is the most important heat source for tropical circulations. Less precipitation means a weakened heat source. Differences between some of the dynamical fields show this weakening (see Fig. 12). Differences between the two simulations of velocity potential at 200 hPa, vertical omega velocity at 500 hPa, and wind vectors at 200 and 700 hPa all show that upward vertical motion, convergence at the lower levels, and divergence at the upper levels decreased for the deforestation case relative to the control case.

The simulated changes in the surface climate for the 3-month averages (1 April–30 June) are even larger for the dry season in southern Amazonia (see Fig. 13). Surface temperatures are warmer by 2°–4°C, precipitation is lower by 1–3 mm day^{-1}, latent heat is reduced by 30–60 W m^{-2} and sensible heat is larger by 20–30 W m^{-2} in the deforestation case relative to the control case for the region south of the equator. It is worth emphasizing that the relative impact of the simulated changes is greatest in the dry season. For instance, the reduction in simulated precipitation in southern Amazonia is about 40%–50% in the dry season for the deforestation case compared to the control case, as opposed to 20%–30% for the annual average (Table 3).

The relative increase in surface temperature and surface albedo calculated for the deforestation case leads to differences in the surface energy budget for the two cases (Table 4). The absorbed solar radiation at the surface is reduced in the deforestation case (186 W m^{-2}) relative to the control case (204 W m^{-2}) because of the higher mean albedo (21.6%) for grassland compared to forest (12.5%) (see Fig. 11c). The higher surface temperature in the deforestation case gives rise to more outgoing longwave radiation from the surface compared to the control case, so that the amount of net radiative energy available at the surface for partitioning into latent and sensible heat flux is considerably smaller in the deforestation case (172 W m^{-2} for the control case and 146 W m^{-2} for the deforested case). Additionally, the smaller green leaf area index and the reduced soil moisture storage capacity in the deforestation case has the effect of reducing the time-averaged transpiration rate; also, in the deforestation case, less precipitation is intercepted and reevaporated, as the surface roughness of the pasture is relatively small. The reduction in transpiration rates and interception losses in the deforestation case implies that a larger proportion of the available net radiative energy goes into sensible heating compared to the forest case; that is, the time-averaged Bowen ratio is 0.62 for the deforested case and only 0.34 for the control case.

The magnitude of the changes in the surface energy budget for the deforested case are more pronounced for the dry season, as shown in Table 4b. Comparing the annual and the seasonal (April–June) mean surface energy budget in Table 4, we see that the magnitude of the differences between the deforested and the control cases are consistently higher for the drier months. For instance, the latent heat flux is now 130 W m^{-2} for the control case (128 W m^{-2} for the annual aver-

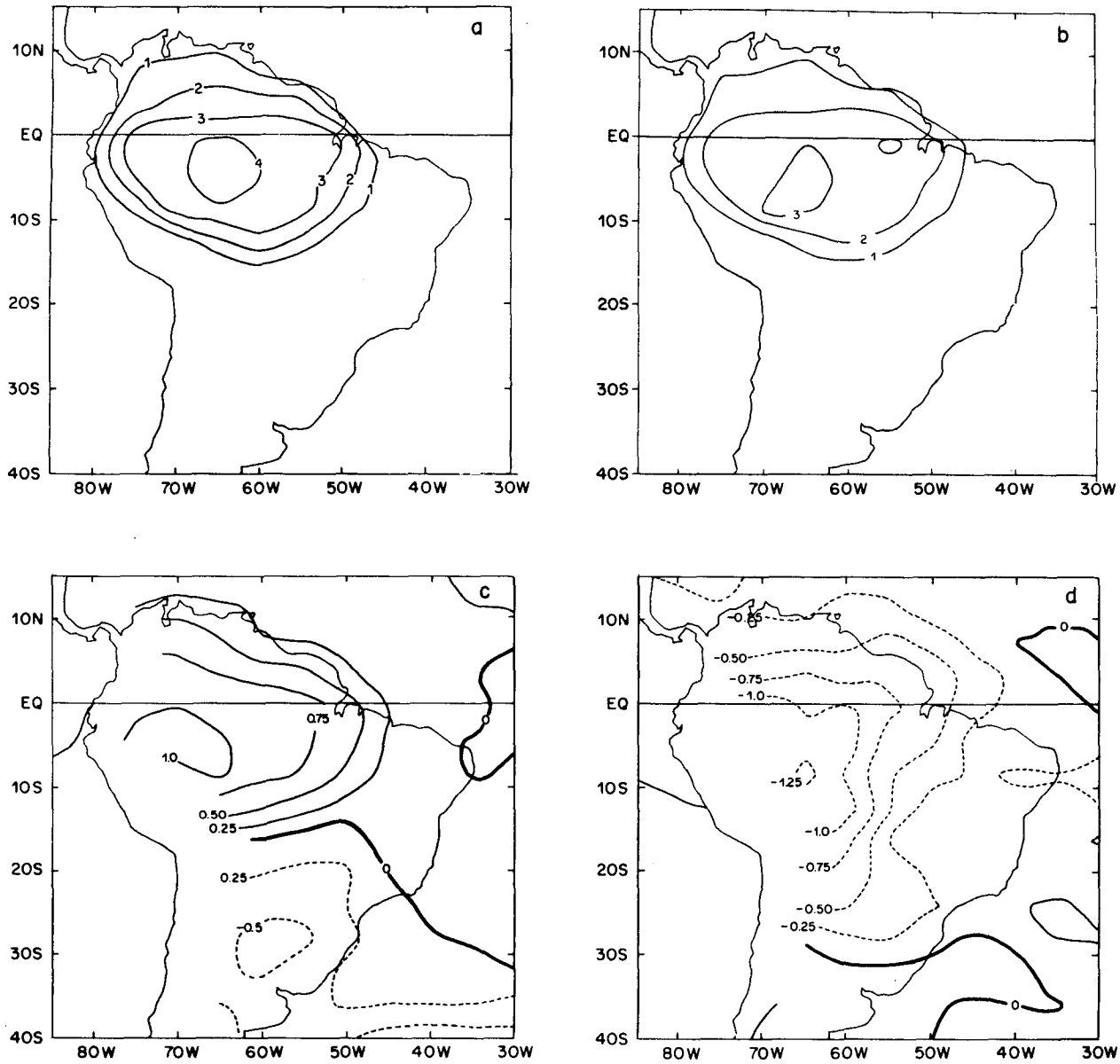

FIG. 10. Differences between 12-month means (January to December) of deforestation and control cases (deforested − control) for South America: (a) deep soil temperature (°C), (b) surface temperature (°C), (c) 850 hPa temperature (°C), (d) 850 hPa specific humidity (g km^{-1}), (e) 850 hPa relative humidity (percent), (f) total precipitation (mm), and (g) sea level pressure (hPa).

age), but only 71 W m^{-2} for the deforested case (90 W m^{-2} for the annual average). The difference in surface temperature between the two simulations is also higher for the dry season (3.3°C) than for the annual average (2.5°C). The bioclimatic consequences of these larger changes during the dry season is discussed in the next section.

The reduction in calculated annual precipitation by 643 mm and in evapotranspiration by 496 mm (Table 3a) suggests that changes in the atmospheric circulation act further to reduce the convergence of moisture flux in the region, a result which could not have been anticipated without the use of a dynamical model of the atmosphere. Higher surface and soil temperatures lead to a slight increase in the sensible heat flux (Fig. 11b); but even the increased warming of the near-surface air and the slight lowering of the surface pressure (Fig. 10g) are not sufficient to increase the convergence of air (and moisture) into the region in the simulation.

As discussed in the Introduction, evapotranspiration

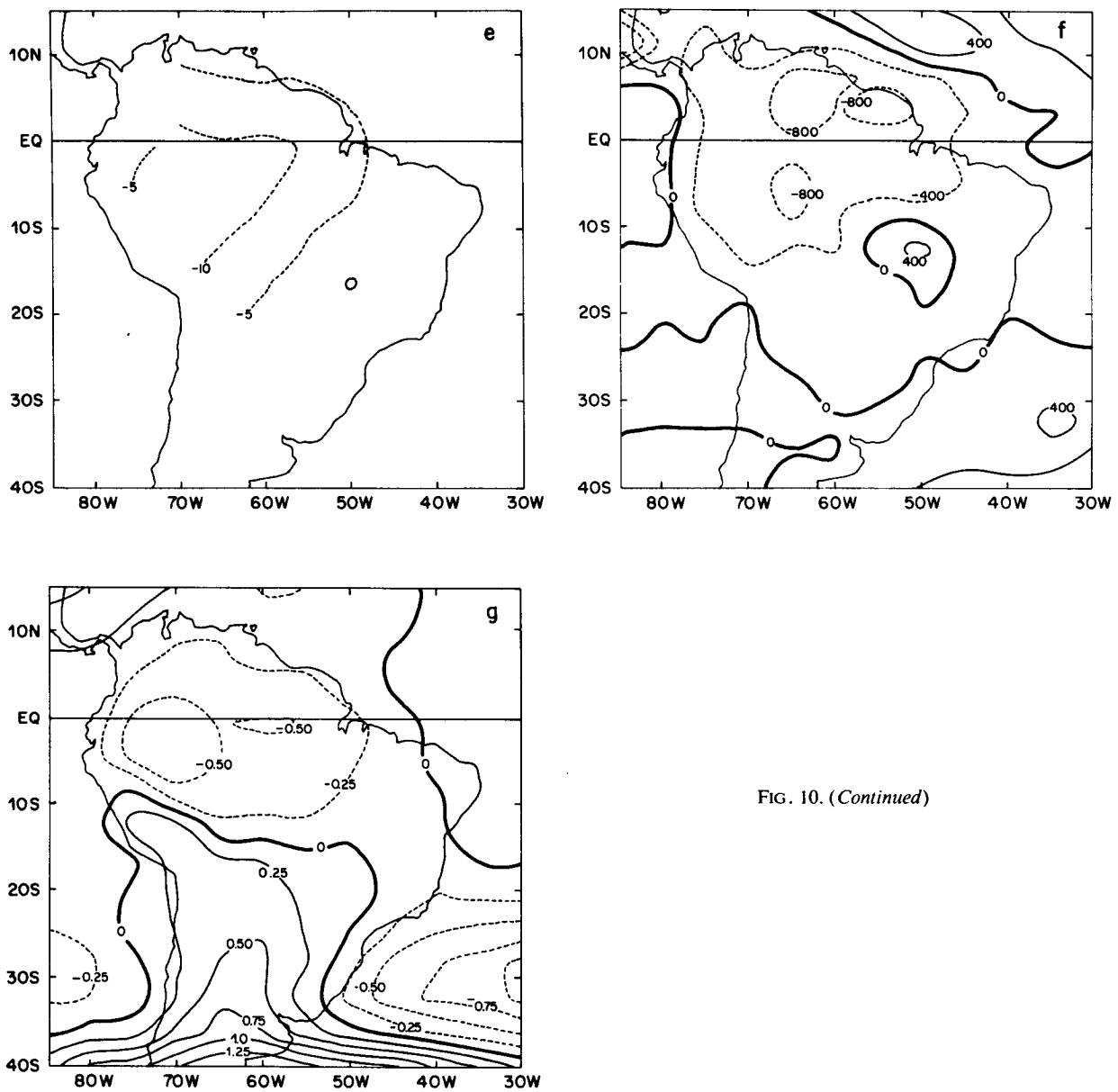

FIG. 10. (*Continued*)

from the forest is one of the important sources of water vapor feeding precipitation in the Amazon. A reduction in evapotranspiration is expected to lead to a reduction in precipitation. However, because of the complexity of the atmosphere–biosphere system and the continuous interactions of dynamical and hydrological processes, a reduction in evaporation might be compensated for by an increase in moisture flux convergence (for instance, if there were a relative lowering of the low-level pressure over Amazonia with respect to the adjacent ocean and a higher flux of moisture into that region). The results of this simulation indicate that such a compensation will not occur for Amazonia and that there is even a further decrease in convergence of the large-scale moisture flux. Only by performing additional experiments and comparing with results from other models will we be able to resolve whether this result is model-dependent. One such comparison can be made with the results of LW. They also found a further decrease of the simulated large-scale moisture convergence (and runoff) when pasture replaced forests in Amazonia.

The changes in soil physical properties following deforestation, notably the decrease in hydraulic conductivity, imply that the surface runoff will increase for the grass cover, primarily immediately after intense

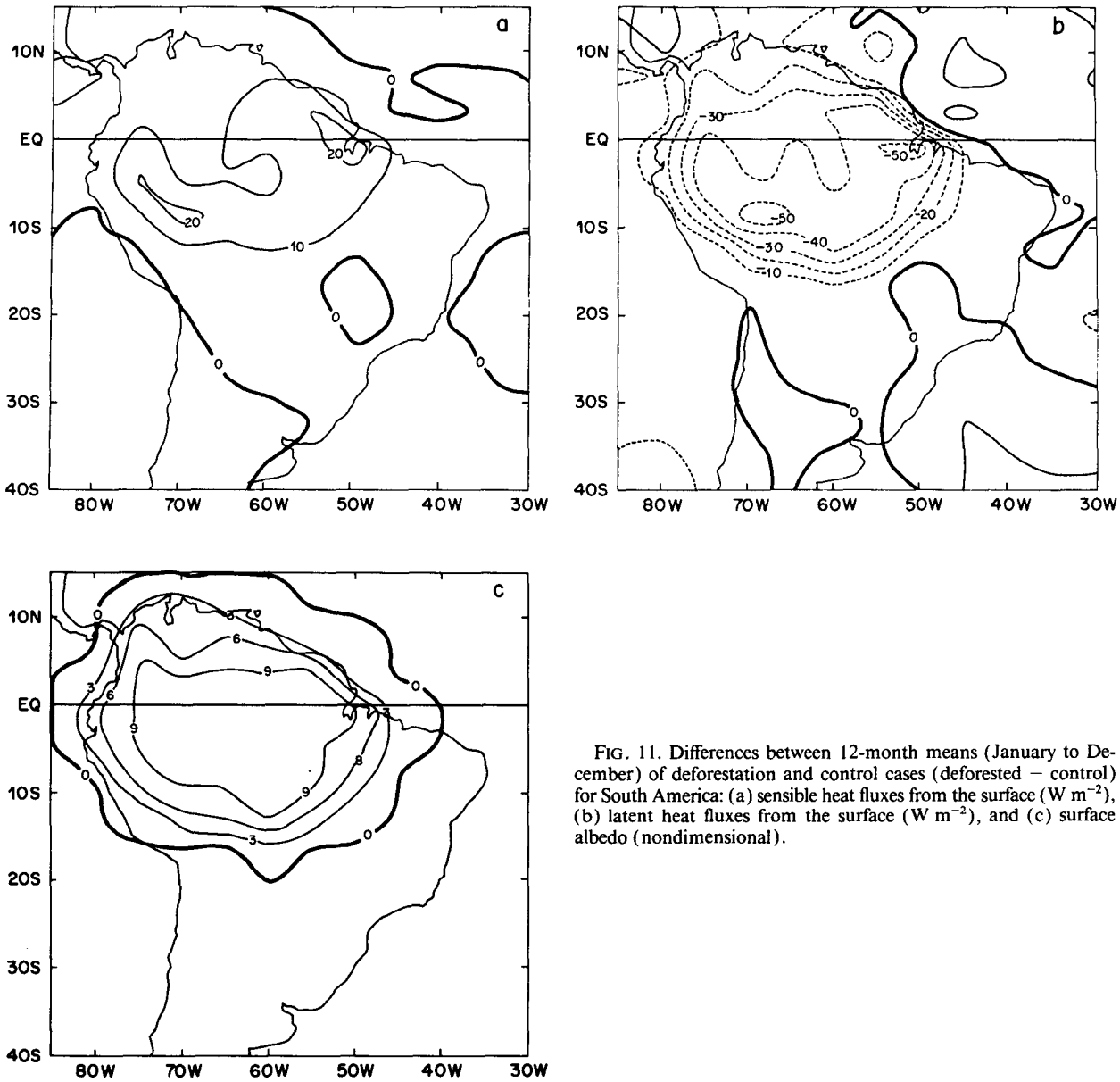

FIG. 11. Differences between 12-month means (January to December) of deforestation and control cases (deforested − control) for South America: (a) sensible heat fluxes from the surface (W m^{-2}), (b) latent heat fluxes from the surface (W m^{-2}), and (c) surface albedo (nondimensional).

storms. There is some limited observational evidence that surface runoff is larger for degraded pasture in Amazonia compared to the surface runoff of nearby forested areas (Fearnside 1988). It is likely that surface runoff would increase for a localized area in which primary forest was replaced by a short vegetation cover. It is also likely that the surface runoff for the Amazon Basin would increase following very large-scale deforestation *if* one can confidently say that precipitation either remained unchanged or increased. However, the results of this simulation and also those of the simulation of LW suggest that the reduction in precipitation rates for the Amazon Basin covered with pasture was larger than the reduction in evapotranspiration, which implied that runoff should actually decrease on the basin scale.

The monthly mean values of surface temperature, precipitation, evapotranspiration, and evapotranspiration minus precipitation for the control and deforestation cases for the total area (Region I + Region II; see Fig. 3 for the definition of Regions I and II) and for Region I and Region II are shown in Figs. 14 and 15, respectively. It can be seen that the differences between the two simulations are consistently of the same sign but of different magnitude for each of the individual months. This consistency is partly a result of the

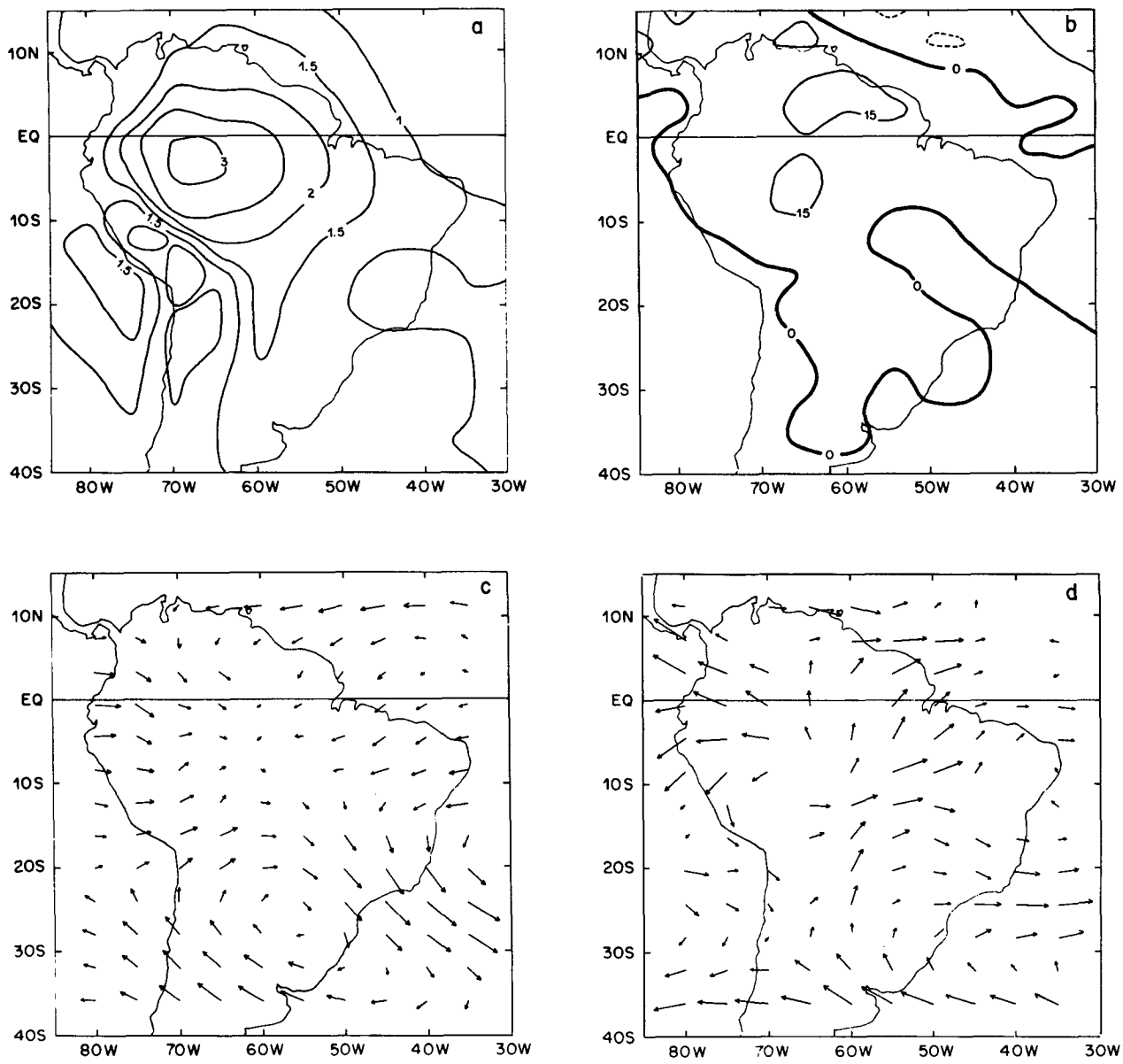

FIG. 12. Differences between 12-month means (January to December) of deforestation and control cases (deforested − control) for South America: (a) 200 hPa velocity potential ($m^2 s^{-1}$), (b) 500 hPa vertical omega velocity (hPa s^{-1}), (c) 200 hPa wind vector differences, and (d) 700 hPa wind vector differences at 700 hPa.

large area used for spatial averaging. As discussed before, the value of evapotranspiration minus precipitation increased in the deforestation simulation. Total runoff was also reduced in the deforestation case because the decrease in precipitation was more than the decrease in evapotranspiration.

c. *Diurnal cycle: Comparison of the two simulations*

Monthly mean diurnal variations of several variables for the months of March (typical of the rainy season) and July (typical of the dry season) for a selected grid point in Amazonia were analyzed to explore the differences between the two cases. The diurnal cycle figures were constructed from averaging the value of a variable for each time step (12 minutes) in the simulation over the selected period. For most of this analysis we selected a grid point in southwestern Amazonia (9.51°S, 66.09°W). All figures of the diurnal cycle show four boxes: the upper boxes are for March and the bottom ones for July; boxes on the left are for the

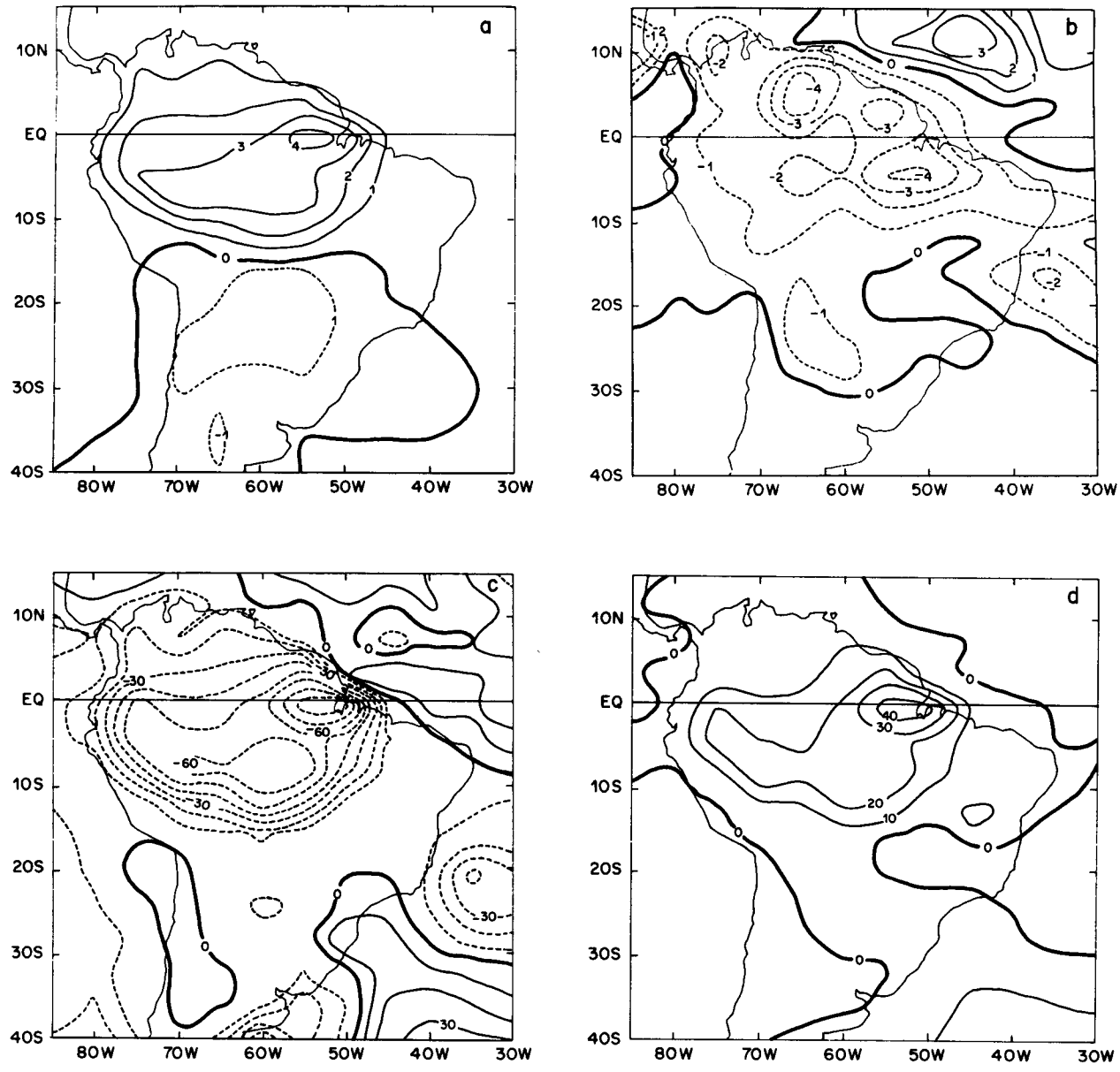

FIG. 13. Differences between 3-month means (April–June) of deforestation and control cases (deforested − control) for South America: (a) surface temperature increase (°C), (b) total precipitation (mm), (c) latent heat fluxes from the surface (W m^{-2}), and (d) sensible heat fluxes from the surface (W m^{-2}).

control simulation and the ones on the right for the deforested simulation.

Both downward shortwave (not shown) and downward longwave radiation are input variables (calculated by the GCM) while SiB calculates upward shortwave (not shown) and longwave fluxes (Fig. 16). Atmospheric longwave radiation calculations in the model are carried out every three hours to give the stepwise shape of downward longwave flux in the figure. Major differences appear in the values of absorbed shortwave radiation flux: the pasture absorbs less solar radiation than the forest due to the higher albedo of the grass cover. The upward longwave radiation is greater in the deforested case due to the higher surface temperature. Therefore, the available net radiation (Fig. 17) is substantially smaller for the deforested case compared to the control case: maximum values of 670 W m^{-2} at 1200 local time for the deforested case as compared to 590 W m^{-2} for the control case.

Less available net radiation at the surface implies

TABLE 3. Mean water budget (a) for the 12-month mean (January–December), and (b) for the 3-month mean (April–June). P is total precipitation [mm yr^{-1} in (a) and mm $month^{-1}$ in (b)]; E is evapotranspiration [mm yr^{-1} in (a) and mm mo^{-1} in (b)]; and PW is precipitable water (mm).

	P	E	$(E-P)$	E/P	PW
		(a) January–December			
Control	2464	1657	−807	0.67	37.7
Deforestation	1821	1161	−660	0.63	35.4
Difference	−643	−496	+147	−0.04	−2.3
Difference in percent	−26.1	−30.0	+18.0	−5.9	−6.1
		(b) April–June			
Control	430	417	−13	0.97	38.2
Deforestation	208	229	+21	1.10	34.9
Difference	−222	−188	+34	+0.13	−3.3
Difference in percent	−51.6	−45.1	+26.1	+13.4	−8.7

differences in the partitioning of energy between latent, sensible, and ground heat fluxes, as seen in Fig. 17. For the forest case, most of the available net energy goes into latent heat flux (evapotranspiration), a smaller portion to the sensible heat flux, and the remaining ground heat flux is very small throughout the day (since the ground is "shielded" by the forest canopy, all fluxes at the ground level are very small). The partition of energy for the control case (lhs of Fig. 17) compares well with the observations of Shuttleworth et al. (1984) for central Amazonia. Latent heat flux is much larger than sensible heat flux for the control case as compared to the deforested case for both March and July. In fact, for this particular grid point, sensible heat flux is larger in magnitude than latent heat flux for the deforested case. Also the diurnal cycle of ground heat flux is more pronounced for the deforested case as more radiation reaches the ground surface through the sparse grass canopy.

It is important to understand the mechanisms that give rise to the large difference between the calculated evapotranspiration rates of the two cases. It can be understood in terms of the smaller values of surface conductance for the grass cover compared to forest (Fig. 18). The maximum surface conductance is a function of the surface soil wetness (a small factor for the tall vegetation but important for grasses) and the amount and type of the green vegetation and its stomatal response to shortwave radiation. The resulting unstressed canopy conductance is a function of vegetation leaf area index, species, and the flux density of PAR. The large difference in the calculated values of maximum canopy conductance for the two treatments is partly due to species differences (field data suggest that the grass leaves, particularly the C_4 species, have much lower conductances), but mainly because of the difference in green leaf area index, nearly 5 for the forest and around 2 for the grass (Table 2). Additionally, the vegetation responds dynamically to changes in the environment to reduce its exposure to desiccation. The controlling environmental factors in SiB that reduce the actual canopy conductance below the maximum value are leaf water potential, surface temperature, and vapor pressure deficit.

In the control case the simulation behaves much as expected, which is reassuring as the physiological parameters were obtained by optimization of the observed fluxes using the same dataset (see Sellers et al. 1989; Shuttleworth et al. 1984). The "unstressed" conductance is more or less symmetric about midday in accordance with the diurnal variation of shortwave radiation. The "stressed" or actual value of the canopy conductance is obtained by multiplying the unstressed value by the factors which account for the effects of leaf water potential, temperature, and local vapor pressure deficit (see Sellers et al. 1986). The vapor pressure deficit effect is dominant: as the air gets drier, the stomates close to reduce the evaporation rate and hence the risk of leaf desiccation, which results in a reduction in conductance. The final stressed conductance (Fig. 18) is therefore asymmetric as the vapor pressure deficit

TABLE 4. Mean surface energy budget (a) for the 12-month mean (January–December), and (b) for the 3-month mean (April–June). Values W m^{-1} [except for a and B (nondimensional) and T_s (°C)]; S is insolation, a is albedo, L_n is net longwave radiation (positive upwards), R_n in available radiative energy, E_t is transpiration plus soil evaporation, E_i is interception loss; E is evapotranspiration ($=E_t + E_i$), H is sensible heating, G is ground heat flux, B is the Bowen ratio (H/E), and T_s is surface temperature.

	S	$(1-a)S$	L_n	R_n	E_t	E_i	E	H	G	B	a	T_s
						(a) January–December						
Control	233	204	−32	172	91	37	128	44	0	0.34	12.5	23.5
Deforestation	237	186	−40	146	64	26	90	56	0	0.62	21.6	26.0
Difference	+4	−18	−8	−26	−27	−11	−38	+12	0	+0.28	+9.1	+2.5
						(b) April–June						
Control	217	190	−30	160	97	33	130	31	−1	0.24	12.4	23.3
Deforestation	220	168	−42	126	52	19	71	55	0	0.77	23.6	26.6
Difference	+3	−22	−12	−34	−45	−14	−59	+24	+1	+0.53	+11.2	+3.3

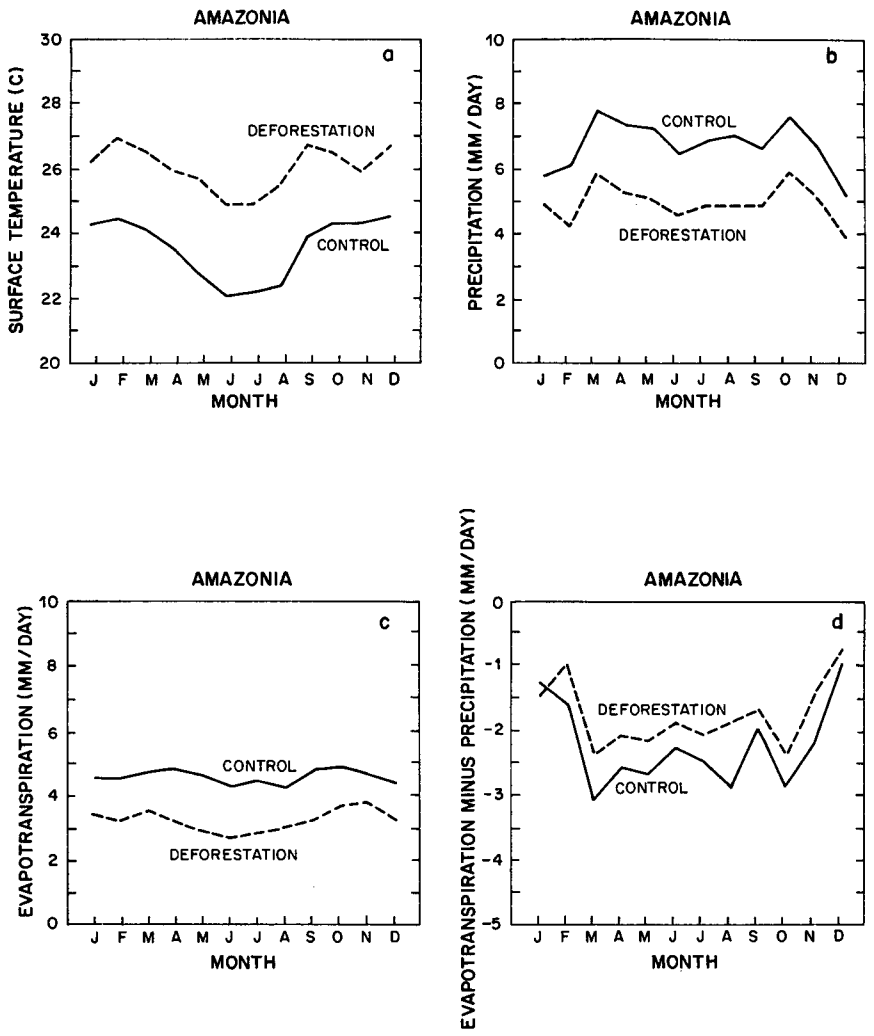

FIG. 14. Monthly distribution (January to December) of the areal average of (a) surface temperature (°C), (b) total precipitation (mm d^{-1}); (c) evapotranspiration (mm d^{-1}), and (d) evapotranspiration minus total precipitation (mm d^{-1}). Solid line is for control case and dashed line is for deforestation case. Areal averages taken over the total area (Regions I + II) marked in Fig. 3.

increases from morning to afternoon. Similar trends can be seen in the grass case except that the vapor pressure deficit term acts to reduce the stressed conductance even more. This is partly due to the higher surface temperature associated with the grass cover, due to its relatively small roughness length, which further increases the local vapor pressure deficit.

Figure 19 shows the diurnal cycle of transpiration and total evaporation (interception loss from canopy and ground cover vegetation plus soil evaporation). It is clear that the large decrease in latent heat flux in Fig. 17 was to a large extent due to the reduction in canopy transpiration for the grass vegetation cover. Interception loss (not shown) was somewhat larger for the forest case, whereas the soil evaporation (not shown) was slightly larger for the deforested case.

In SiB, precipitation is intercepted and stored on the vegetation. The diurnal cycle of the canopy water store for the two simulations is depicted in Fig. 20. During the night, the atmospheric stability near the surface impedes all evaporation. During the day, the aerodynamic resistance decreases and the intercepted water evaporates freely. Comparing the values for the two simulations, one sees, as expected, that the water stored for the grass vegetation cover is much smaller than the water store for the forest.

The diurnal cycle of total precipitation (convective plus large-scale) and total evapotranspiration (Fig. 21) shows that total precipitation is larger than total evapotranspiration for the control case during March, that is, during the rainy season. During the dry season, precipitation is smaller than evapotranspiration for the

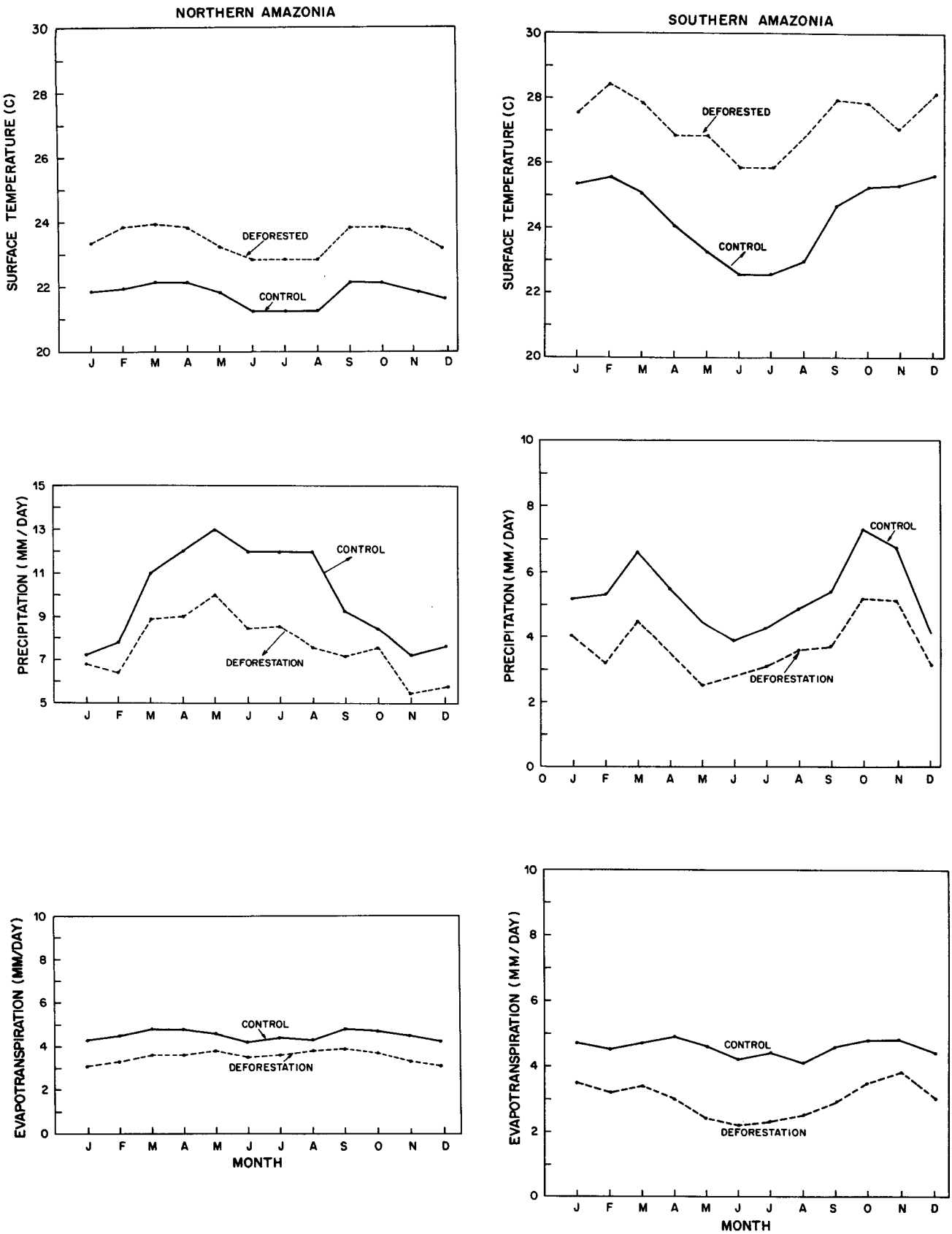

FIG. 15. Monthly distribution (January to December) of the areal average of surface temperature (°C) (top diagrams), total precipitation (mm d^{-1}) (center diagrams), and evapotranspiration (mm d^{-1}) (bottom diagrams). Solid line is for control case and dashed line is for deforestation case. Areal averages taken over Region I (northern Amazonia) and Region II (southern Amazonia) marked in Fig. 3.

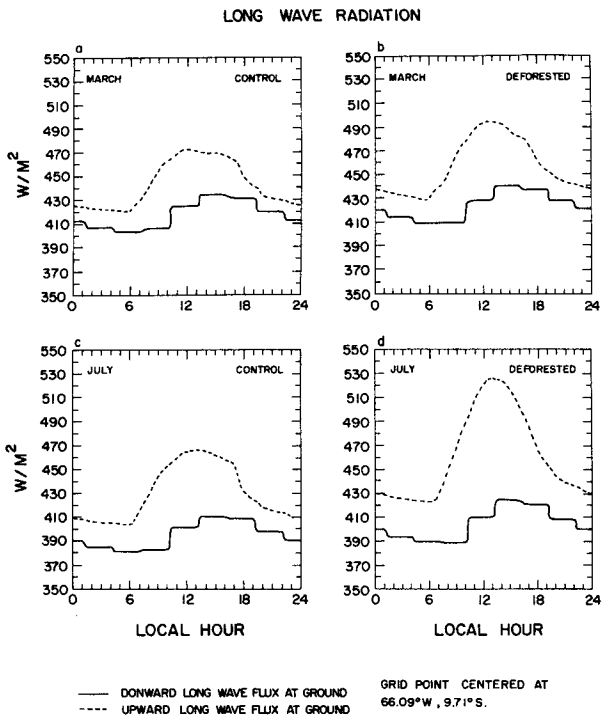

FIG. 16. Diurnal cycles of calculated longwave radiation fluxes (W m^{-2}) at the surface. All figures for the diurnal cycle refer to a grid point located at 9.71°S, 66.09°W and are shown for March (rainy season) and July (dry season) for both control and deforested simulations.

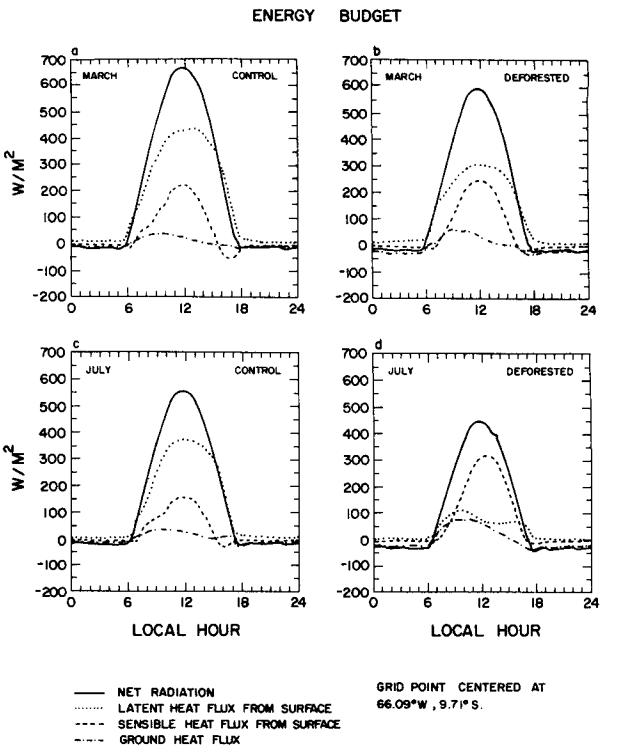

FIG. 17. Diurnal variation of surface energy fluxes, showing available net radiation, latent heat flux, sensible heat flux, ground heat flux (W m^{-2}).

control case. For the deforested case, precipitation and evapotranspiration are very small for the dry season.

The diurnal cycles of canopy, ground, and deep soil temperatures and the temperature of the lowest atmospheric level are depicted in Fig. 22. Diurnal amplitude of canopy and ground temperatures are much higher for the deforested simulation (13°C) than for the control simulation (8°C) for March. (During the dry season this contrast is even higher: 16°C versus 7.5°C.) Also, the maximum and minimum temperatures are always higher for the deforested simulation. It is interesting to note that the air temperature at the lowest model layer falls off more slowly during night hours for the deforested case. The larger atmospheric stability near the surface is a result of the low surface roughness of the grass cover. As a result of the higher surface temperatures, the relative humidity for the deforested case shows smaller midday values (60% for the forested case as opposed to 50% for the deforested case) as shown in Fig. 23.

Finally, the diurnal cycle of the magnitude of the surface stress is shown in Fig. 24. The values of total surface stress are consistently higher in the forest case, a result that can be accounted for by the decreased roughness length of the grass cover.

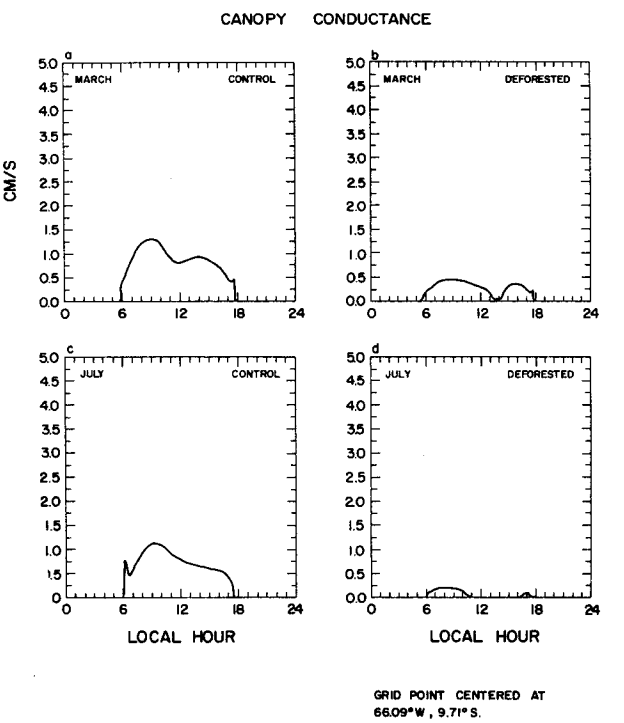

FIG. 18. Diurnal variation of canopy conductance (cm s^{-1}).

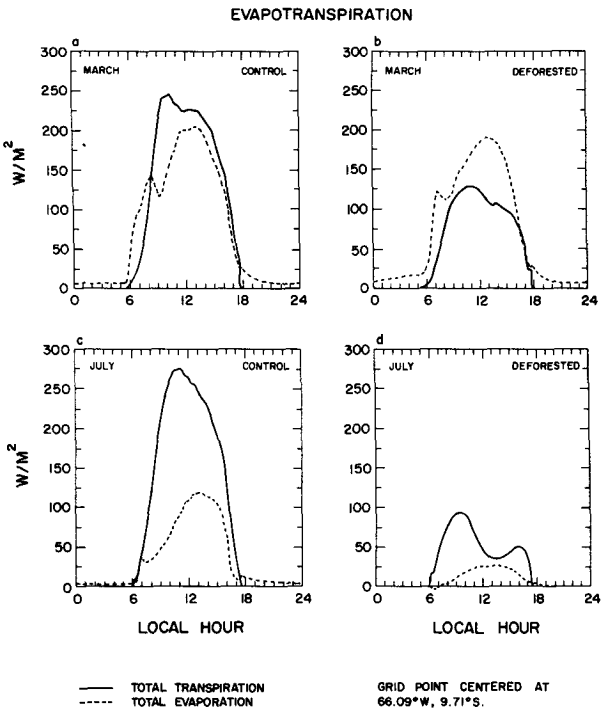

FIG. 19. Diurnal variation of transpiration and total evaporation (W m^{-2}).

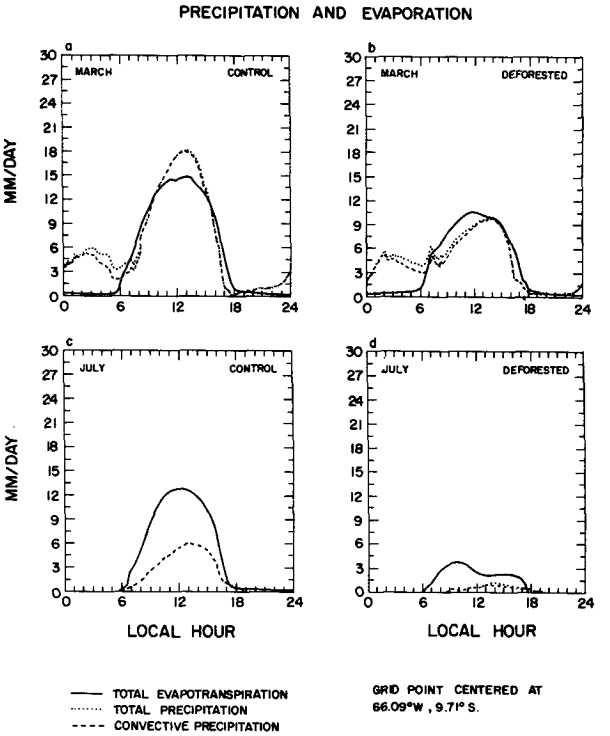

FIG. 21. Diurnal variation of total precipitation (convective plus large-scale precipitation) and total evapotranspiration (mm d^{-1}).

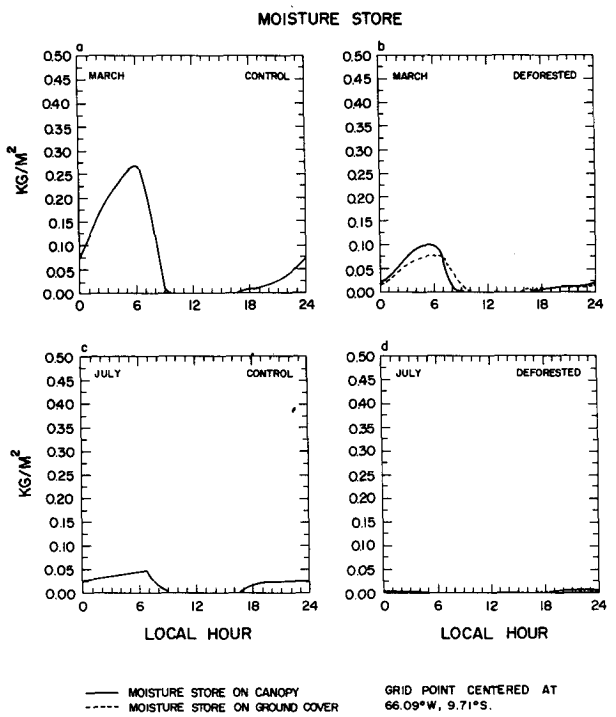

FIG. 20. Diurnal variation of canopy water storage and ground vegetation water storage (mm).

5. Discussion

Let us ask the question: Does the meteorological record show any changes that could be attributed to tropical deforestation? Amazon streamflow integrates the effect of rainfall over a large area of tropical forest and thus might show the effects of man-induced changes in the hydrological cycle. To date, almost 90 years of riverflow data for a point near Manaus have shown only what appears to be natural variability (Richey et al. 1989). Even the tendency toward higher water levels in the Amazon River from 1964 through 1976, which Gentry and Lopes-Parody (1981) ascribed to deforestation, was shown to be a result of large-scale precipitation changes at decadal time scales (Rocha et al. 1989). However, on the local scale, deforestation has been shown to cause significant changes in the surface and subsurface climate for a site in Nigeria (Lawson et al. 1981) and for a site in Surinam (Schulz 1960).

The average low-level airflow over tropical South America east of the Andes (Chu and Hastenrath 1982) shows that moisture flow is directed from Amazonia toward central Brazil. Thus the water vapor available for precipitation in central Brazil comes mostly from Amazonia; any change in the water vapor transport could conceivably affect precipitation in that region, even when one considers that the main rain-producing mechanisms in the area are due to frontal systems mov-

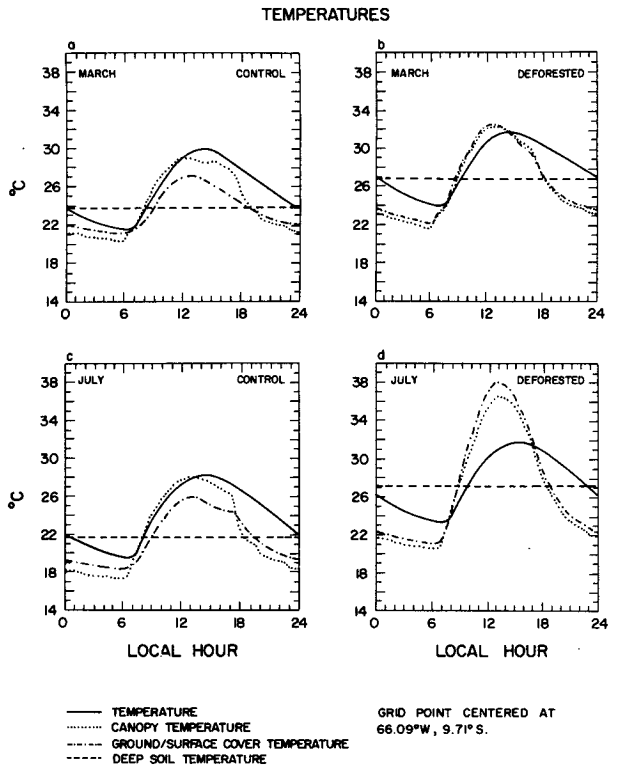

FIG. 22. Diurnal variation of deep soil temperature, ground temperature, canopy temperature, and air temperature at the lowest model layer in C.

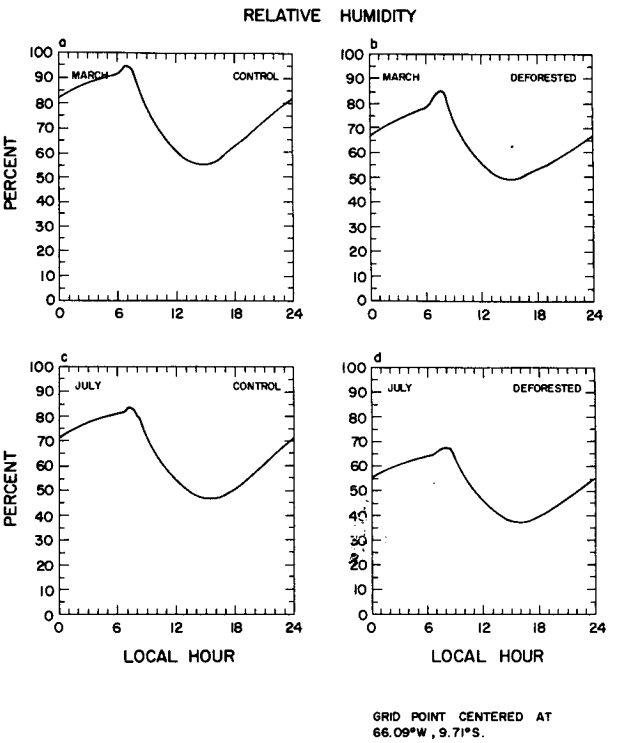

FIG. 23. Diurnal variation of relative humidity (percent).

ing in from the midlatitudes of the Southern Hemisphere. Our model results have shown a smaller decrease in precipitation in central Brazil due to deforestation. That decrease, however, could not be attributed to a smaller southward moisture flux from Amazonia since that flux did not change appreciably; specific humidity decreased but wind speed increased slightly.

Another point of interest is the large precipitation rate simulated in western Amazonia. On average, the atmospheric column in that area apparently has more water vapor than near the Atlantic coast (as supported by the Amazonian Boundary Layer Experiment-ABLE 2B measurements). The Atlantic Ocean, of course, provides the major supply of water vapor to Amazonia. Considering that western Amazonia is between 2000 and 3000 km inland from the main oceanic water vapor source, recycling of water vapor through evapotranspiration is clearly very important. A decreased water vapor flux to the west, as in the model results, might imply decreased precipitation in those areas, even in the absence of large-scale deforestation there. It is also important to mention that the very high precipitation rates observed on the eastern Andean slopes (up to 5 m annually on the Peruvian and Colombian Andean slopes) must be related not only to the mechanical

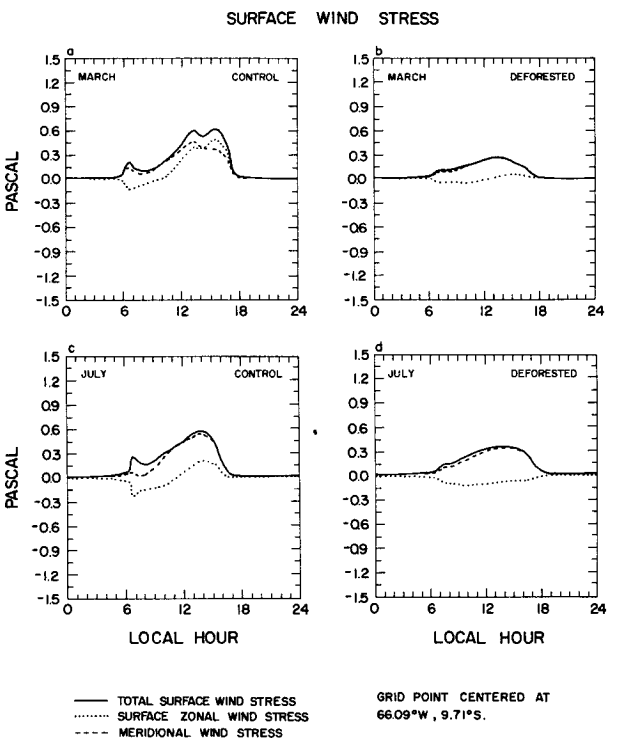

FIG. 24. Diurnal variation of zonal, meridional, and total surface stress (Pa).

uplifting of the airflow but also to the amount of moisture being transported. The maintenance of these very high precipitation rates and the resulting lack of a dry season is thought to be an important factor supporting the tremendous species diversity—reportedly the largest in the world—in Colombian Amazonia. Therefore, even small changes in the precipitation regimes of the eastern Andean slopes could have profound effects on species diversity in that area.

A few significant changes in global circulation were also evident in the deforestation simulation, especially over North America; however, climatic fluctuations over the northern midlatitudes are generally large in nature as well as in simulations even without any forced perturbations, and thus the anomalies cannot be definitely linked to deforestation. Moreover, the artificial constraint of time-invariant SST fields makes it difficult to draw any definitive conclusions about the global effects of Amazon deforestation from this study.

As mentioned in the Introduction, reconstruction of the paleoclimate record (Dickinson and Virji 1987; Whitmore and Prance 1987) shows evidence of periods with a drier, colder climate for the Amazon, such as during the peak of the last Ice Age, about 18 000 yr BP. The tropical forest retreated considerably and much of Amazonia was covered by savanna, indicating that the forest–savanna boundary responds to the external forcing provided by the general circulation of the atmosphere over very long time scales.

However, the rain forest possesses some unique characteristics with respect to its interactions with the atmosphere, such as low albedo, high rates of evapotranspiration and nutrient recycling, large roughness to the surface airflow, and large water-holding capacity of soils. These characteristics combine to maintain, in principle, a higher level of precipitation than would exist otherwise with a different type of vegetation such as savanna. Considering that evergreen rain forests exist only in places where monthly precipitation is not less than about 100 mm in the driest months (Prance 1986), these characteristics act as positive feedback for maximizing the forest's chance of survival; that is, the forest–atmosphere interaction acts in the direction of perpetuating the forest. Of course, there are limits to the power of this effect. The maintenance of the forest is under the primary control of the general circulation of the atmosphere since there is a limit to the rainforest-induced increase in precipitation; our study suggests that this limit is of the order 20% to 30% when compared to a grassy vegetation cover. Now the transition areas (forest to savanna) to the east, south, and north of Amazonia, where the dry season is longer and more pronounced, would be the first to be affected by a drier climate following massive deforestation. These are the areas where intense clearings are taking place (southern and southwestern Amazonia).

Interannual variability of precipitation in Amazonia is large, as revealed by the river streamflow record. A large part of this variability is linked to El Niño–Southern Oscillation (ENSO) events (Richey et al. 1989; Nobre and Oliveira 1986). There are also reports showing that during severe dry spells in Amazonia extensive forest fires can occur (ref. cited in Sternberg 1987; Sanford et al. 1985). These infrequent, intense, and long dry spells are usually linked to the simultaneous occurrence of intense ENSO episodes (Nobre and Nobre 1991). However, the forest appears to be adapted to withstand these large interannual variations in precipitation and the sporadic occurrence of forest fires. Even at the boundaries of the forest, where the interannual variability is more pronounced, migration of the forest border is not observed.

A discussion on the ecological implications of the model's predicted changes is appropriate. The predicted decrease of precipitation, evapotranspiration, relative humidity, and increase of surface temperature, accompanied by a lengthening of the dry season, might imply that a different type of vegetation would be in equilibrium with the climate simulated for the deforestation case, most likely a savannalike vegetation such as the "cerrado" of central Brazil. Two characteristics of such vegetation make it particularly adapted to the foreseeable new climate: it can endure a 6-month dry season and it is fire-adapted. [Actually, fire plays an important role in its ecology in the same way as it does for the savanna vegetation to the north of the rainforest, the Gran Sabana, in Venezuela (Sanford et al. 1985; Sternberg 1987).]

A number of ecological factors are important in maintaining the forest in place in addition to climatic considerations. These include the complexity and intensity of interspecies relationships (e.g., association of particular tree species with particular insect or vertebrate pollen or seed vectors), the dynamics of gap exploitation by young emerging trees, and the maintenance of soil microclimate and physical environment (warm, moist, well-structured soil) conducive to a dense and active soil fauna population, ranging from bacteria and fungi to earthworms and beetles. All of these ecological factors are vulnerable to changes in climate, but they are also very sensitive to the forest patch size; it has been demonstrated that below a minimum patch size, complex ecological communities rapidly "lose" species and disintegrate to less diverse and more vulnerable communities. Clearly, then, it is not only the extent but the geometry of the deforestation that is important in terms of the future of the tropical forest biome.

Returning to our simulation results, it is interesting to speculate on what type of natural vegetation would replace the degraded pasture if the anthropogenic influence were withdrawn. The southern boundary of the forest with the cerrado is thought to be determined by soil moisture deficits and fire frequency. We will

use next the control simulation to develop a climatological criterion for defining the forest–cerrado boundary and then apply this criterion to the deforestation simulation to calculate the post-deforestation bioclimatic boundary. Note that this methodology is fixed to the *relative* differences between the two simulations and not to the control model's performance with respect to the observed climate; this procedure should remove some of the effects of model bias.

We have assumed that the length and intensity of the dry season determine the forest–cerrado boundary through a series of interacting factors, including ecological competition, fire frequency, pollination vector survivability, etc. The vegetation responds to changes in soil moisture tension rather than changes in the evapotranspiration or precipitation regime directly. It is therefore useful to calculate a soil moisture stress index that is directly related to the physiology of the tropical forest. Equation (1) is based on the stomatal stress factor, $f(\varphi)$, used in SiB to calculate the canopy conductance response to extreme (negative) soil moisture tensions (see appendix A for details on the effect of soil moisture stress on the vegetation evapotranspiration rate as calculated in SiB):

$$I = \frac{1}{T_E - T_0}\int_{T_0}^{T_E} \frac{\varphi_r - \varphi_2}{\varphi_1 - \varphi_2}\,dt; \quad 0 \leqslant \frac{\varphi_r - \varphi_2}{\varphi_1 - \varphi_2} \leqslant 1 \quad (1)$$

I stress index; $0 < I < 1$

φ_r soil moisture potential in the root zone, m

φ_1, φ_2 leaf water potentials at which the tropical forest vegetation stomates start to close and are completely closed, m

T_0, T_E time of beginning, end of dry season (1 June, 31 August), respectively.

Note that I varies between 1, where soil moisture stress in the dry season would have no impact on canopy conductance or photosynthesis ($\varphi_r > \varphi_1$), and 0, where both conductance and photosynthesis are zero and the tropical forest vegetation could not survive.

Fields of the index I were calculated by numerically integrating Eq. (1) for the gridpoint daily values of φ_r and are displayed in Fig. 25. North–south transacts of I are shown in Fig. 26; it appears that the *current* tropical forest–cerrado boundary is associated with values of I of around 0.5 in the control case, at which point it can be assumed that the forest is out-competed by drought-tolerant, fire-resistant cerrado species. In Fig. 27, the deforestation case fields of I have been analyzed to derive the new bioclimatological boundary ($I = 0.5$) between the forest and cerrado. Note that the boundary has moved north by roughly 500 to 1000 km in parts of the southern Amazon Basin in response to the changes in evapotranspiration, precipitation, runoff, and soil physical properties in the deforestation case.

The procedure outlined above is simple, and

(i) takes account of model bias in precipitation and evapotranspiration climatologies by correlating the control model value of soil moisture stress index, I, with the observed forest–cerrado boundary, and

(ii) directly addresses the effects of soil moisture stress on the tropical forest cover by relating the soil moisture tension, φ_r, rather than wetness, to the critical parameters used to limit evapotranspiration and photosynthesis, φ_1 and φ_2.

The result shown in Fig. 27 implies that after large-scale deforestation, the tropical forest could not easily reestablish itself below the $I = 0.5$ contour even if the anthropogenic pressure were subsequently removed. To a significant extent, then, tropical deforestation would be effectively irreversible in a large region of the Amazon Basin: regrowth would depend on the presence of forest in the northern half of the basin followed by

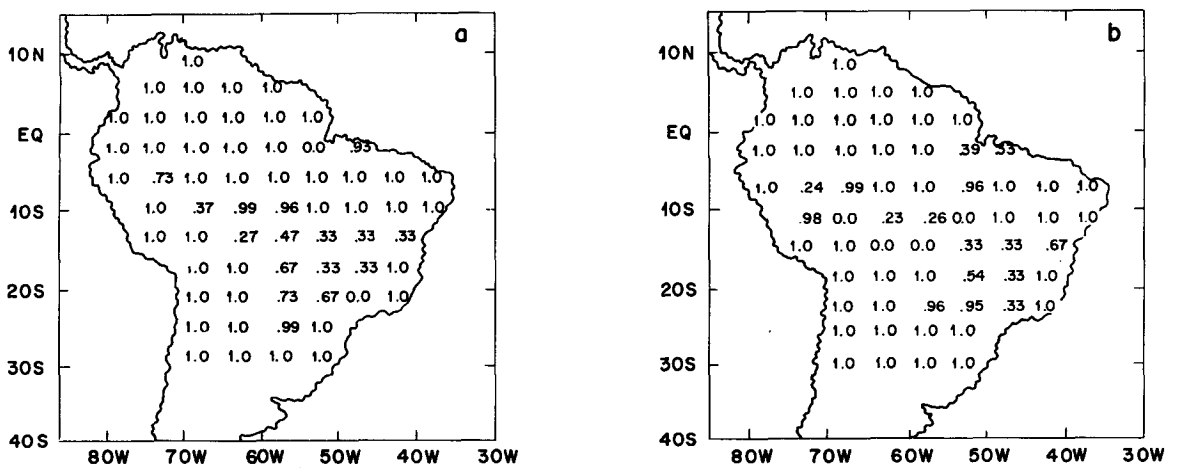

FIG. 25. Gridpoint values of soil moisture stress index for June/August, for (a) control and (b) deforested cases; see Eq. (1) in text.

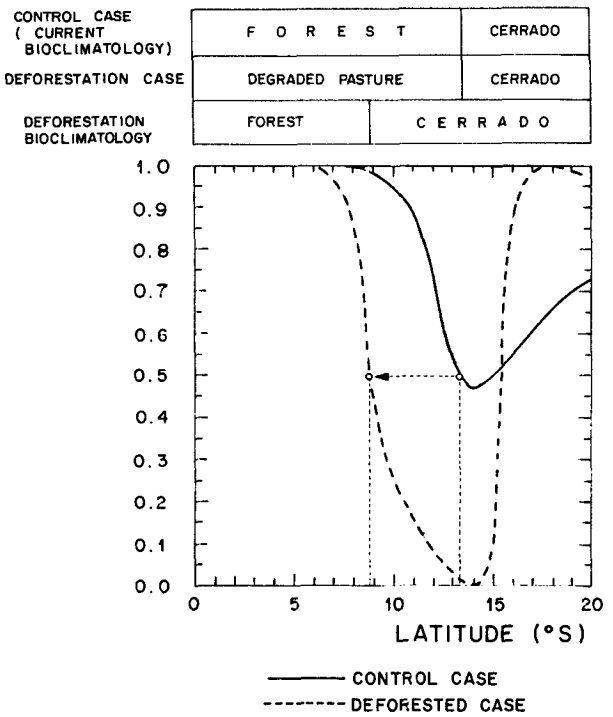

FIG. 26. Soil moisture index, I (see definition in the text), plotted as a north–south transect for 55°W/60°W longitude. Critical value of $I = 0.5$ moves north in deforestation case. Blocks above show distribution of vegetation types for the transect: (top) control case and/or assumed current bioclimatology; (middle) deforestation case (prescribed); (bottom) bioclimatology associated with deforestation case.

a gradual southern movement of the forest southern boundary as the entire climatological–hydrological–ecological system moved slowly back to its predeforestation equilibrium state. The time scale for such a process would be limited by the time scale of ecological succession, that is, centuries to millennia.

6. Concluding remarks

The conversion of tropical forest into pastures or other types of short vegetation is occurring at ever-increasing rates in Amazonia, as well as in other tropical forests of the world. It is almost certain that this conversion will cause changes in the microclimate of the disturbed areas. If the size of the perturbed area is sufficiently large, even the regional climate may be altered.

In this study the effect of a large-scale deforestation of Amazonia on climate has been investigated using a realistic coupled atmosphere–biosphere model. The model was integrated for one year with a representation of the tropical forests now covering Amazonia (control case) and then for one year with the forest replaced by a degraded pasture (deforested case). Differences between the two model simulations have been interpreted as the possible result of Amazonia deforestation. It was found that the surface temperature in the deforested region increased by 1°–3°C, evapotranspiration decreased by 20%–40%, and precipitation decreased by 20%–30%. Comparative measurements of the diurnal cycle of canopy and subsurface temperature at cleared and forested sites in Ibadan, Nigeria (Lawson et al. 1981) and in Surinam (Schulz 1960) showed a large increase of soil (5°C) and air (3°C) temperatures for the cleared areas compared to the forested ones. On the other hand, basin-scale changes of the Amazonia hydrology that could be attributed to deforestation have not been detected to date (Rocha and Nobre 1989). This may be because as yet only a relatively small area has been cleared (approximately 11% of the tropical forest had been cleared in Brazilian Amazonia by 1989).

A significant result of this study is the simulated reduction in precipitation over Amazonia, which is larger than the corresponding regional reduction in evapotranspiration, implying that the dynamical convergence of moisture flux also decreased as a result of deforestation. The spatial and temporal coherence of the decrease in precipitation implies that the deforested case is associated with a longer dry season. The lack of an extended dry season apparently sustains the current tropical forests, and therefore a lengthening of the dry season could have serious ecological implications (Le Houerou and Popov 1978; Lauer 1989; Hamilton 1989). Among other effects, the frequency and intensity of forest fires could increase significantly and the life cycles of pollination and seed distribution vectors could be perturbed.

These results suggest that a complete and rapid destruction of the Amazon tropical forest could be effectively irreversible in the southern part of Amazonia. Changes in the region's hydrological cycle and the disruption of complex plant–animal relations could be so profound that once the tropical forests were destroyed, they might not be able to reestablish themselves.

A bioclimatic scheme was proposed that defines the position of the rainforest–cerrado boundary to the south and north of Amazonia. This scheme was based on calculating a time-integrated soil moisture stress index appropriate to the tropical forest and relating the spatial fields of that quantity to the current position of the forest–cerrado boundary. The methodology was then applied to the deforestation simulation results to provide an initial estimate on how much the natural boundary would retreat with the new simulated equilibrium climate. The results indicate that the post-deforestation bioclimatic boundary between these vegetation types could be quite different from the present-day case. The new bioclimatological boundary between the forest and cerrado would move north by roughly 500 to 1000 km in parts of the southern Amazon Basin in response to changes in evapotranspiration, precip-

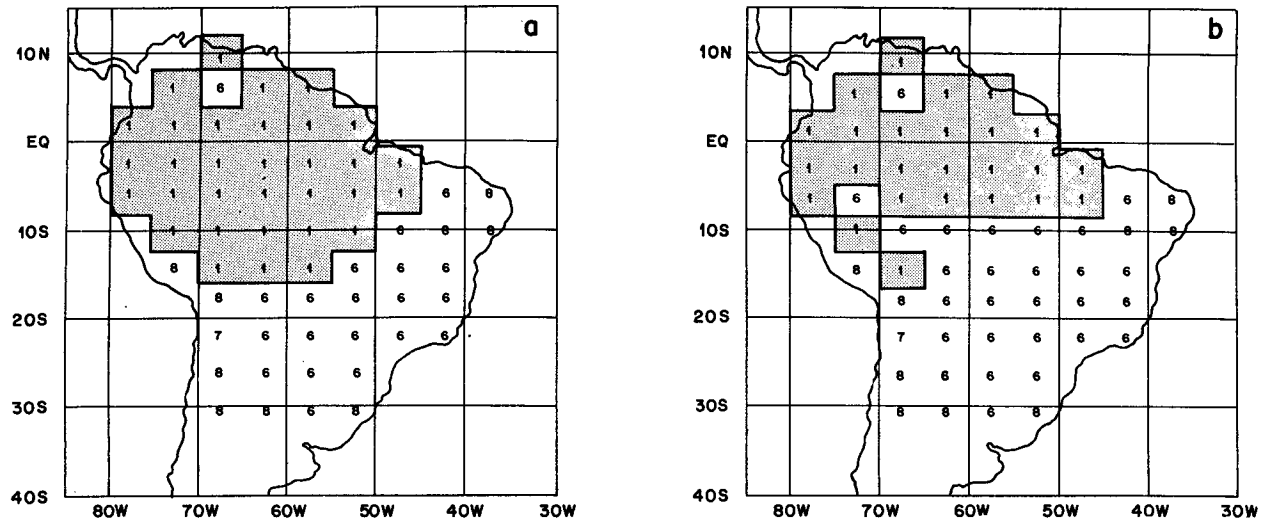

FIG. 27. Bioclimatology for the control case (a, current bioclimatology) associated with deforestation (b, revised bioclimatology after deforestation such as the analysis of the vegetation stress index fields shows). The shaded area with "1" is tropical forest, "6" refers to cerrado. The forest boundary is depicted by the heavy solid line.

itation, runoff, and soil physical properties following deforestation.

So far we have focused our attention only on the Amazonian tropical forest. What can we say about climatic impacts caused by removal of tropical forests in equatorial Africa and Southeast Asia? It is likely that the effects will be quite similar at the microclimate level: higher near-ground temperatures and larger diurnal fluctuations of temperature and humidity deficit, increased runoff during rainy periods and decreased runoff during the dry season, decreased soil moisture, and possibly decreased evapotranspiration. Can we say anything about changes in precipitation? The answer is a complex one. For Southeast Asia large-scale changes in precipitation are less likely since the precipitation climate of that area of the western Pacific and Indian oceans is apparently controlled by large-scale features. On one hand, the precipitation distribution responds to the high sea surface temperatures (SST > 28°C) that are conducive to large rates of evaporation as well as a tendency for the low-level air to converge from areas of lower SST to areas with higher SST; these two factors account for the high precipitation. On the other hand, land–sea heating contrasts drive the monsoonal circulations of Southeast Asia and the associated heavy rainfall.

However, in Africa there is some possibility that the removal of the tropical forest might affect the regional climate. A biophysical feedback mechanism, as proposed by Charney et al. (1977), might cause an enhancement in aridification along the northern and southern boundaries of the forest. For reasons similar to the ones discussed in this study, changes in albedo, surface roughness, and soil moisture caused by replacement of forest by overgrazed pasture would result in decreased precipitation. This could, in turn, induce further clearings deeper into the forest. However, this question is not settled yet because interannual and longer-term rainfall variability in tropical Africa is apparently also connected to planetary-scale phenomena, notably global SST distributions (Folland and Palmer 1986).

Acknowledgments. We thank J. Kinter, L. Marx, M. Fennessy, and E. Schneider for help in conducting this simulation experiment, H. Rocha and P. Dirmeyer for help in the processing and diagnosis of model outputs, and A. D. Nobre for providing information about the Amazonian ecosystem. We also thank A. C. Fonseca for help in the preparation of the manuscript and A. L. Oliveira and A. L. Silva for drafting the final figures. This research was supported by National Science Foundation Grant ATM-87-13567 and National Aeronautical and Space Administration Grants NAGW-1269, NAG 5-892, and NAGW-557. The first author was partly supported by the Brazilian Space Research Institute (INPE).

APPENDIX

The Soil Moisture Stress Index

In SiB the effect of soil moisture stress on the vegetation evapotranspiration rate (and hence the photosynthetic rate) is given by:

$$g_c = g_c^* [f(\delta_e) \cdot f(T) \cdot f(\varphi)] \qquad \text{(A1)}$$

g_c = canopy conductance, m s^{-1}
g_c^* = unstressed canopy conductance, m s^{-1}

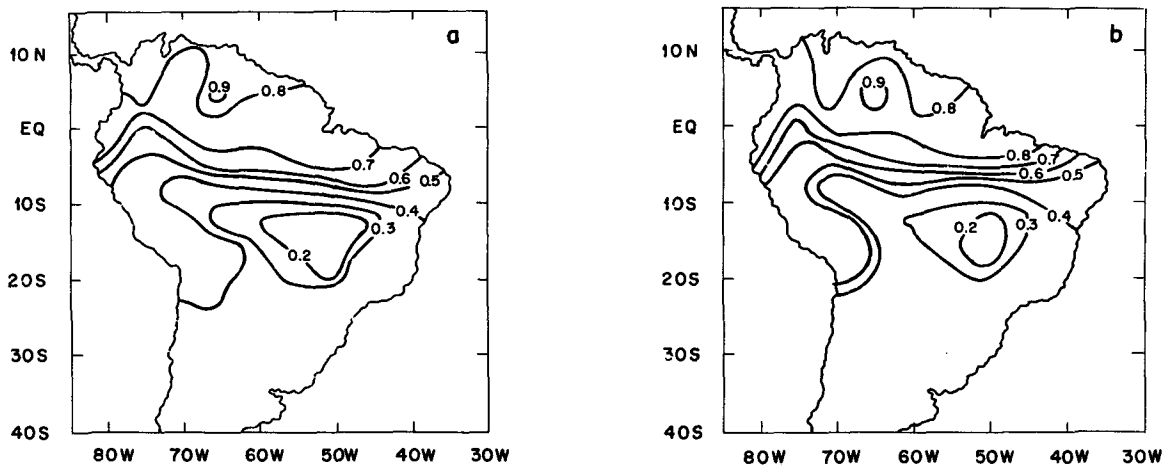

FIG. A1. Simulated fields of root zone soil wetness (W_2) for August: (a) control and (b) deforested cases (values were smoothed before plotting).

$f(\delta_e), f(T), f(\varphi)$ = stress factors accounting for the effects of vapor pressure deficit (δ_e), temperature (T), and leaf water potential (φ), respectively.

The stress factors, $f(x)$, are described in detail in Sellers et al. (1986); all vary between 1 (no stress) and 0 (extreme stress causing complete stomatal closure and a shutdown of photosynthesis).

The leaf water potential stress factor is given by

$$f(\varphi) = \frac{\varphi - \varphi_2}{\varphi_1 - \varphi_2} \qquad \text{(A2)}$$

φ = canopy leaf water potential, m
φ_1, φ_2 = leaf water potentials at which stomates start to close and are completely closed, m.

The leaf water potential is calculated using the catenary scheme of Federer (1979) whereby

$$E = \frac{[\varphi_r - \varphi]}{r_{\text{soil}} + r_{\text{plant}}} \rho_w \qquad \text{(A3)}$$

φ_r = soil moisture potential in the root zone, m
$r_{\text{soil}}, r_{\text{plant}}$ = resistance to passage of water through soil pores and plant vascular system, respectively, s m^{-1} (see Sellers et al. 1986)
ρ_w = density of water, kg m^{-3}.

The root zone soil moisture potential φ_r, is calculated from the SiB soil moisture layer 2 wetness value.

$$\varphi_r = \varphi_s W_2^{-B} \qquad \text{(A4)}$$

φ_s = soil moisture potential at saturation, m
B = empirical parameter
W_2 = wetness of root zone (soil layer 2)

Equations (A1) through (A4) represent a closed system when $g_c = f(\varphi, \cdots)$ is used to calculate the

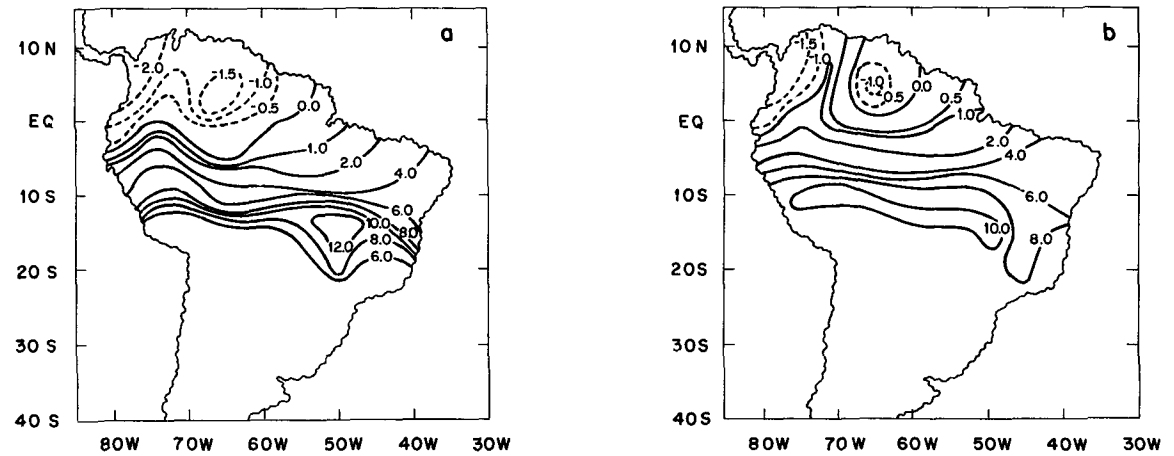

FIG. A2. Simulated fields of soil moisture potential in the root zone (cologarithm values) for August: for control (left) and deforested (right) cases (values were smoothed before plotting).

evaporation rate. Thus, when soil moisture stress is limiting ($\varphi_r < \varphi_1$) transpiration, conductance and photosynthesis are strong functions of φ_r and less strongly related to the evaporative demand.

Figure A1 shows the simulated fields of root zone soil wetness for the end of the dry season (August) for the two cases; there is little that can be learned from a comparison of these two figures, as the vegetation is calculated to be responsive to soil moisture tension, not wetness. Figure A2 compares the equivalent soil tension values for the two runs; note that there is a marked increase in the area of drier soils (represented by high positive values of the cologarithm of soil tensions in the figure) in the deforestation case. This result is partially due to the change in soil properties in the deforestation case, in particular the increase in the B parameter as the soil disaggregates and becomes more claylike. An increase in B significantly increases φ_r and thus has the effect of reducing the amount of soil moisture ($\varphi_r > \varphi_2$) available to the vegetation.

REFERENCES

Bjorkman, O., 1981: Responses to different quantum flux densities. *Physiological Plant Ecology I: Responses to the Physical Environment,* O. I. Lange, P. S. Nobel, C. B. Osmond and H. Zirgles, Eds., Springer-Verlag, 57–107.

Brasil, Instituto de Pesquisas Espaciais, 1989: Avaliação da cobertura florestal na Amazônia Legal utilizando Sensoriamento Remoto Orbital. INPE, São José dos Campos, SP, Brazil.

Brasil, Ministério de Minas e Energia, 1980: Projeto RADAM. Mapas de Vegetação. Departamento Nacional de Produção Mineral, Rio de Janeiro, RJ, Brazil.

Budyko, M. I., 1974: *Climate and Life.* Academic Press, 508 pp.

Buschbacher, R., C. Uhl, and E. A. S. Serrao, 1988: Abandoned pastures in eastern Amazonia. II. Nutrient stocks in the soil and vegetation. *J. Ecol.,* **76,** 682–699.

Camillo, P. J., and R. J. Gurney, 1986: A resistance parameter for bare-soil evaporation models. *Soil Sci.,* **142**(2), 95–105.

Charney, J. G., W. J. Quirk, S. H. Chow, and T. Kornfield, 1977: A comparative study of the effects of albedo change on drought in semi-arid regions. *J. Atmos. Sci.,* **34,** 1366–1388.

Chauvel, A., M. Grimaldi, and D. Tessier, 1988: Examples of soil transformation following deforestation and plantation in the Central Amazon Basin (Brazil): Changes in pore volume and size and consequences for their water-bearing properties. *Proc. Conf. on the Amazonian Tropical Forest.*

Chu, P-S., and S. Hastenrath, 1982: Atlas of upper-air circulation over tropical South America. Dept. Of Meteorology, University of Wisconsin, Madison, 237 pp.

Cohen, J. C. P., M. A. F. Silva Dias, and C. A. Nobre, 1989: Aspectos climatologicos das linhas de instabilidade na Amazônia. *Climanálise,* **4**(11), 34–40.

Colinvaux, P. A., 1987: Amazon diversity in light of the paleoecological record. *Quat. Sci. Rev.,* **6,** 93–114.

——, 1989: The past and future Amazon. *Sci. Amer.* **260,** 102–109.

Crutzen, P., and Andreae, M. A., 1990: Biomass burning in the tropics: Impact on atmospheric chemistry and biogeochemical cycles. *Science,* (submitted).

Davies, R., 1982: Documentation of the solar radiation parameterization in the GLAS Climate Model. NASA Tech. Memo 83961, 57 pp.

Dias, A. C. C. P., and P. Nortcliff, 1985: Effect of two land-clearing methods on the physical properties of an Oxisol in the Brazilian Amazon. *Trop. Agric.,* **62,** 207–212.

Dias Filho, M. B., 1987: Especies forrageiras e estabelecimento de pastagens na Amazônia. EMBRAPA-CPATU Tech. Rep., Belém, PA, Brazil, 49 pp.

Dickinson, R. E., 1984: Modelling evapotranspiration for three-dimensional global climate models. *Climate Processes and Climate Sensitivity, Geophys. Monogr.,* No. LF29, Am. Geophys. Union, 58–72.

——, 1989a: Modeling the effects of Amazonian deforestation on a regional surface climate: A review. *Agric. For. Meteor.,* **47,** 339–348.

——, 1989b: Implications of tropical deforestation for climate: A comparison of model and observational descriptions of surface energy and hydrological balance. *Phil. Trans. R. Soc. London B.*

——, and H. Virji, 1987: Climate change in the humid tropics, especially Amazonia, over the last thousand years. *The Geophysiology of Amazonia,* R. E. Dickinson, Ed., Wiley, 91–105.

——, and A. Henderson-Sellers, 1988: Modelling tropical deforestation: A study of GCM land-surface parameterizations. *Quart. J. Roy. Meteor. Soc.,* **114,** 439–462.

——, ——, P. J. Kennedy, and M. F. Wilson, 1986: Biophere–atmosphere transfer scheme (BATS) for the NCAR Community Climate Model. Tech. Note TN-275 + STR, National Center for Atmospheric Research, Boulder, CO.

Dorman, J. L., and P. J. Sellers, 1989: A global climatology of albedos, roughness length, and stomatal resistance for atmospheric general circulation models as represented by the Simple Biosphere Model (SiB). *J. Appl. Meteor.,* **28,** 833–855.

Fearnside, P. M., 1982: Deforestation in the Brazilian Amazon: How fast is it occurring? *Interciencia,* **4,** 220–225.

——, 1987a: Causes of deforestation in the Brazilian Amazon. *The Geophysiology of Amazonia,* R. E. Dickinson, Ed., Wiley, 37–61.

——, 1987b: Summary of progress in quantifying the potential contribution of Amazonian deforestation to the global carbon problem. *Proc. of the Workshop on Biogeochemistry of Tropical Rain Forests: Problems and Research,* D. Athie, T. E. Lovejoy and P. de M. Oyens, Eds., University of Sao Paulo, Centro de Pesquisa de Energia Nuclear na Agricultura (CENA), 75–82.

——, 1988: An ecological analysis of predominant land uses in the Brazilian Amazonia. *The Environmentalist,* **8.**

——, 1990: The rate and extent of deforestation in Brazilian Amazonia. *Environ. Conserv.,* (in press).

——, A. T. Tardin, and L. G. Meira Filho, 1990: Deforestation rate in Brazilian Amazônia. INPE, São José dos Campos, SP, Brazil.

Federer, C. A., 1979: A soil-plant atmosphere model for transpiration and availability of soil water. *Water Resour. Res.,* **15.3,** 555–562.

Figueroa, S. N., and C. A. Nobre, 1990: Precipitation distribution over central and western tropical South America. *Climanálise,* **5**(6), 36–40.

Folland, C. K., and T. N. Palmer, 1986: Sahel rainfall and worldwide surface temperature. *Nature,* **320,** 602–607.

Franken, W., and P. R. Leopoldo, 1984: Hydrology of a catchment area of central Amazonian forest streams. *The Amazon: Limnology and Landscape Ecology of a Mighty Tropical River and its Basin,* H. Sioli, Ed., W. Junk, Dordrecht.

Gentry, A. H., and J. Lopes-Parody, 1980: Deforestation and increased flooding in the upper-Amazon. *Science,* **210,** 1354–1356.

Ghuman, B. S., and R. Lal, 1987: Effects of deforestation on soil properties and microclimate of a high rain forest in southern Nigeria. *The Geophysiology of Amazonia,* R. E. Dickinson, Ed., Wiley, 225–244.

Godbole, R. V., and J. Shukla, 1981: Global Analysis of January and July sea-level pressure. NASA Tech. Memo 82097.

Hamilton, A., 1989: *Ecosystems of the World: Tropical Rain Forest Ecosystems.* Vol. 14B. Elsevier, 155–182.

Harshvardhan and T. G. Corsetti, 1984: Longwave radiation parameterization for the UCLA/GLAS GCM. NASA Tech. Memo 86072, 65 pp.

Harshvardhan, R. Davies, D. A. Randall, and T. G. Corsetti, 1987: A fast radiation parameterization for general circulation models. *J. Geophys. Res.*, **92**, 1009–1016.

Henderson-Sellers, A., and V. Gornitz, 1984: Possible climatic impacts of land cover transformations, with particular emphasis on tropical deforestation. *Clim. Change*, **6**, 231–258.

Houghton, R. A., R. D. Boone, J. M. Melillo, C. A. Palm, G. M. Woodwell, N. Myers, B. Moore, and D. L. Skole, 1985: Net flux of CO_2 from tropical forests in 1980. *Nature*, **316**, 617–620.

Jarvis, P. G., 1976: The interpretation of the variations in leaf water potential and stomatal conductance found in canopies in the field. *Philos. Trans. R. Soc. London. Ser. B.*, **273**, 593–610.

Jerry, H., 1986: The soil resource: Origin and behavior. *Ecological Studies 37*, 3d ed., Springer-Verlag, 377 pp.

Jordan, C. F., 1984: Soil of the Amazon rainforest. *Amazonia*, G. T. Prance and T. E. Lovejoy, Eds., Pergamon Press, Chapter 5, 83–94.

Justice, C. O., J. R. G. Townshend, B. N. Holben, and J. C. Tucker, 1985: Analysis of the phenology of global vegetation using meteorological satellite data. *Int. J. Remote Sens.*, **6**, 1271–1318.

Kinter, J. L., J. Shukla, L. Marx, and E. K. Schneider, 1988: A simulation of the winter and summer circulations with the NMC Global Spectral Model. *J. Atmos. Sci.*, **45**, 2486–2522.

Korner, C., J. A. Scheel, and M. Bauer, 1979: Maximum leaf diffusive conductance in vascular plants. *Photosynthetica*, **3**(1), 45–82.

Kousky, V. E., 1979: Frontal influences in Northeast Brazil. *Mon. Wea. Rev.*, **107**, 1140–1153.

——, 1980: Diurnal rainfall variation in Northeast Brazil. *Mon. Wea. Rev.*, **108**, 488–498.

Kuo, H. L., 1965: On the formation and intensification of tropical cyclones through latent heat release by cumulus convection. *J. Atmos. Sci.*, **22**, 40–63.

Lacis, A. A., and J. E. Hansen, 1974: A parameterization for the absorption of solar radiation in the Earth's atmosphere. *J. Atmos. Sci.*, **31**, 118–133.

Lauer, W., 1989: *Ecosystems of the World: Tropical Rain Forest Ecosystems.* Vol. 14B. Elsevier, 7–54.

Lawson, T. L., R. Lal, and K. Oduro-Afriyie, 1981: Rainfall redistribution and microclimatic changes over a cleared watershed. *Tropical Agriculture Hydrology*, R. Lal, and E. W. Russel, Eds., John Wiley & Sons, 141–151.

Lean, J., and D. A. Warrilow, 1989: Climatic impact of Amazon deforestation. *Nature*, **342**, 311–313.

Le Houerou, H. N., and G. F. Popov, 1978: *An Ecoclimate Classification of Intertropical Africa.* Food and Agriculture Organization.

Lettau, H., K. Lettau, and L. C. B. Molion, 1979: Amazonia's hydrologic cycle and the role of atmospheric recycling in assessing deforestation effects. *Mon. Wea. Rev.*, **107**, 227–238.

Ludlow, M. M., and G. L. Wilson, 1971a: Photosynthesis of tropical pasture plants. I: Illuminance, carbon dioxide concentration, leaf temperature, and leaf–air vapour pressure difference. *Aust. J. Biol. Sci.*, **24**, 449–470.

——, and G. L. Wilson, 1971b: Photosynthesis of tropical pasture plants. II. Temperature and illuminance history. *Aust. J. Biol. Sci.*, **24**, 1065–1075.

——, and K. Ibaraki, 1979: Stomatal control of water loss in Siratro (*Macroptilium atropurpureum* (DC) Urb.), a tropical pasture legume. *Ann. Bot.*, **43**, 639–647.

——, M. J. Fisher, and J. R. Wilson, 1985: Stomatal adjustment to water deficits in three tropical grassed and a tropical legume grown in controlled conditions and in the field. *Aust. J. Plant Physiol.*, **12**, 131–149.

Malingreau, J. P., and C. J. Tucker, 1988: Large-scale deforestation in the southern Amazon Basin of Brazil. *Ambio*, **17**, 49–55.

Manabe, S., 1969: The atmospheric circulation and hydrology of the earth's surface. *Mon. Wea. Rev.*, **97**, 739–774.

Matthews, E., 1985: Atlas of archived vegetation, land-use, and seasonal albedo datasets. NASA Tech Memo. 86199, 54 pp.

Medina, B. F., 1985: Influencia de dois metodos de preparo de area na compactacao de um latossolo amarelo no Estado do Amazonas. *Anais do II Simpósio do Trópico Umido*, Belem, EMBRAPA-CPATU, 446–455.

Mellor, G. L., and T. Yamada, 1982: Development of a turbulence closure model for geophysical fluid problems. *Rev. Geophys. Space Phys.*, **20**, 851–875.

Mintz, Y., 1984: The sensitivity of numerically simulated climates to land-surface conditions. *The Global Climate.* J. T. Houghton, Ed., Cambridge University Press, 79–106.

Miyakoda, K., and J. Sirutis, 1986: Manual of the E-physics. [Available from the authors at Geophysical Fluid Dynamics Laboratory, Princeton University, P.O. Box 308, Princeton, NJ 08542.]

Molion, L. C. B., and R. L. G. Dallarosa, 1990: Pluviometria da Amazônia: São os dados confiáveis? *Climanálise*, **5**(3), 37–41.

Monin, A. S., and A. M. Obukhov, 1954: Basic laws of turbulent mixing in the ground layer of the atmosphere. *Akad. Nauk SSSR Geofiz. Inst. Tr.*, **151**, 163–187.

Mori, T., and G. T. Prance, 1987: Species diversity, phenology, plant-animal interaction, and their correlation with climate, as illustrated by the Brazil nut family (*Lecythidaceae*). *Geophysiology of Amazonia.* R. E. Dickinson, Ed., John Wiley & Sons, 64–69.

Myers, N., 1982: Depletion of tropical moist forests: A comparative review of rates and causes in the three main regions. *Acta Amazônica*, **12**, 745–758.

Nepstad, D. C., and Uhl, C., 1990. Seedling environment in mature forest and old fields of eastern Amazonia: Light, temperature, water and nutrients. *J. Ecol.*, (submitted).

Ng, T. T., J. R. Wilson, and M. M. Ludlow, 1975: Influence of water stress on water relations and growth of a tropical (C_4) grass, *Panicum maximum var. trichoglume. Aust. J. Plant Physiol.*, **2**, 581–595.

Nobre, C. A., 1983: Amazonia and climate. *Proc. of the WMO Technical Conf. on Climate for Latin America and the Caribbean*, Colombia, WMO, 409–416.

——, and A. S. Oliveira, 1986: Precipitation and circulation anomalies in South America and the 1982–83 El Niño–Southern Oscillation episode. Preprints, *Proc. Second Int. Conf. on Southern Hemisphere Meteorology*, New Zealand, Amer. Meteor. Soc., 442–445.

——, and P. Nobre, 1991: The 1926 drought in Amazonia. *Climanálise*, (in press).

Oliveira, A. S., and C. A. Nobre, 1986: Interactions between frontal systems in South America and tropical convection over the Amazon. Preprints, *Proc. Second Int. Conf. on Southern Hemisphere Meteorology*, New Zealand, Amer. Meteor. Soc., 56–59.

Philips, N., 1979: The nested grid model. NOAA Tech. Rep. NWS-22, 79 pp.

Potter, G. L., H. W. Ellsaesser, M. C. MacCracken, and F. M. Luther, 1975: Possible climatic impact of tropical deforestation. *Nature*, **258**, 697–698.

Prance, G. T. 1986: Tropical rain forests and the world atmosphere. *AAAS Sel. Symp. Ser.*, **101**.

——, and T. E. Lovejoy, Eds., 1984: *Amazonia.* Pergamon Press.

Richey, J. E., C. A. Nobre, and C. Deser, 1989: Amazon River discharge and climate variability: 1903 to 1985. *Science*, **246**, 101–103.

Rocha, H. R., C. A. Nobre, and M. C. Barros, 1989: Variabilidade natural de longo prazo no ciclo hidrológico da Amazônia. *Climanálise*, **4**(12), 36–43.

Rowntree, P., 1988: Review of general circulation models as a basis for predicting the effects of vegetation change on climate. *Proc. of the United Nations University Workshop on Forest, Climate, and Hydrology: Regional Impacts*, United Nations University, Tokyo.

Salati, E., and P. B. Vose, 1984: Amazon basin: a system in equilibrium. *Science*, **225**, 129–138.

——, and C. A. Nobre, 1991: Possible climatic impacts of tropical deforestation. *Clim. Change*, in press.

Salo, J., 1987: Pleistocene forest refuges in the Amazon: Evolution

of the biostratigraphical, lithostratigraphical, and geomorphological data. *Ann. Zool. Fennici,* **24,** 203–211.

Sanford, Jr., R. L., J. Saldarriaga, K. E. Clark, C. Uhl, and R. Herrera, 1985: Amazon rain-forest fires. *Science,* **227,** 53–55.

Sato, N., P. J. Sellers, D. A. Randall, E. K. Schneider, J. Shukla, J. L. Kinter III, Y-T Hou, and E. Albertazzi, 1989a: Effects of implementing the Simple Biosphere Model in a general circulation model. *J. Atmos. Sci.,* **46,** 2757–2782.

——, ——, ——, ——, ——, ——, ——, and ——, 1989b: Implementing the Simple Biosphere Model (SiB) in a general circulation model: Methodologies and results. NASA Contractor Rep. 185509, 76 pp.

Sela, J. G., 1980: Spectral modeling at the National Meteorological Center. *Mon. Wea. Rev.,* **108,** 1279–1292.

Sellers, P. J., and J. L. Dorman, 1987: Testing the Simple Biosphere Model (SiB) using point micrometeorological and biophysical data. *J. Climate Appl. Meteor.,* **26,** 622–651.

——, Y. Mintz, Y. C. Sud, and A. Dalcher, 1986: A Simple Biosphere Model (SiB) for use within general circulation models. *J. Atmos. Sci.,* **43,** 505–531.

——, W. J. Shuttleworth, J. L. Dorman, A. Dalcher, and J. M. Roberts, 1989: Calibrating the Simple Biosphere Model for Amazonian tropical forest using field and remote sensing data. Part I: Average calibration with field data. *J. Appl. Meteor.,* **28,** 727–759.

Shubart, H. O. R., 1977: Critérios ecológicos para o desenvolvimento agrícola das Teras Firmes dà Amazônia. Publ. INPA, Manaus, Amazonas, Brazil, 29 pp.

Shu Fen Sun, 1982: Moisture and heat transport in a soil layer forced by atmospheric conditions. M.S. thesis, Dept. of Civil Engineering, University of Chicago, 72 pp.

Shukla, J., and Y. Mintz, 1982: The influence of land-surface evapotranspiration on the earth's climate. *Science,* **215,** 1498–1501.

——, C. A. Nobre and P. J. Sellers, 1990: Amazonia deforestation and climate change. *Science,* **247,** 1322–1325.

Shulz, J. P., 1960: *Ecological Studies on Rain Forest in Northern Surinam.* 270 pp.

Shuttleworth, W. J., 1988: Evaporation from Amazonian rain forest. *Proc. Roy. Soc. London Ser. B,* **233,** 321–346.

——, and R. E. Dickinson, 1989: Comments on "Modelling tropical deforestation: A study of GCM land-surface parameterizations." *Quart. J. Roy. Meteor. Soc.,* **115,** 1177–1179.

——, J. H. C. Gash, C. R. Lloyd, J. Roberts, A. O. Marques Filho, G. Fish, V. P. Silva Filho, M. N. G. Ribeiro, L. C. B. Molion, C. A. Nobre, L. D. A. Sá, O. M. R. Cabral, S. R. Patel, and J. C. Moraes, 1984: Eddy correlation measurements of energy partition of Amazon forest. *Quart. J. Roy. Meteor. Soc.,* **110,** 1143–1162.

Skole, D. L., W. Chomentowski, and C. A. Nobre, 1990: New estimates of Amazonian deforestation in the late 1970s using a Geographic Information System. Center for Complex Systems Research, University of New Hampshire, Durham.

Sternberg, H. O'R., 1987: Aggravation of floods in the Amazon river as a consequence of deforestation? *Geogr. Ann.,* **69A,** 201–220.

Sud, Y. C., and A. Molod, 1988: A GCM simulation study of the influence of Saharan evapotranspiration and surface-albedo anomalies on July circulation and rainfall. *Mon. Wea. Rev.,* **116,** 2388–2400.

Tiedke, M., 1984: The effect of penetrative cumulus convection on the large-scale flow in a general circulation model. *Beitr. Phys. Atmos.,* **57,** 216–239.

Uhl, C., R. Buschbacher, and E. A. S. Serrao, 1988: Abandoned pastures in eastern Amazonia. I: Patterns of plant succession. *J. Ecol.,* **76,** 663–681.

Whitmore, T. C., and G. T. Prance, 1987: *Biogeography and Quaternary History in Tropical America.* Oxford University Press.

Wilding, L. P., N. E. Smeck, and G. F. Hall, eds., 1983: Pedogenesis and soil taxonomy. LFII: The soil orders. *Developments in Soil Science,* Vol. LF11b, Elsevier, 410 pp.